PTEP

Prog. Theor. Exp. Phys. **2012**, 01A108 (31 pages)
DOI: 10.1093/ptep/pts033

Selected results in lattice quantum chromodynamics

Z. Fodor[1,2,3,*]

[1]*Department of Physics, University of Wuppertal, D-42119 Wuppertal, Germany*
[2]*Jülich Supercomputing Centre, Forschungszentrum Jülich, D-52425 Jülich, Germany*
[3]*Institute for Theoretical Physics, Eötvös University, H-1117 Budapest, Hungary*
*E-mail: fodor@physik.uni-wuppertal.de

Received July 10, 2012; Accepted July 23, 2012; Published November 14, 2012

The results of the Budapest–Marseille–Wuppertal Collaboration are summarized. Both $T = 0$ and $T > 0$ findings are presented. Special emphasis is put on the "physical point" (which is used to describe results with physical quark masses extrapolated all the way to the continuum limit). At $T = 0$, the light hadron spectrum, F_K/F_π, the quark masses, and the kaon bag parameter are discussed. At $T > 0$, results for the nature of the quantum chromodynamics transition, the transition temperature, the equation of state (both at vanishing and nonvanishing chemical potentials), the curvature of the phase diagram, and the effects of magnetic fields are discussed. All these results are full results (representing findings at physical quark masses in the continuum limit).

1. Introduction

Lattice quantum chromodynamics (QCD) is the most systematic tool to understand the nonperturbative regime of strong interactions. It has a long history going back to the early 1970s. Lattice gauge theory was introduced in Ref. [1]. (The independent developments of Smit and Polyakov were never published; see, e.g., Ref. [2].) Recent overviews can be found in Refs. [3–9]. (See also the classic introductory text of Ref. [10].) After almost forty years, lattice QCD entered a new era. Today, we have several full results for various physical questions. These full answers represent results at physical quark masses (directly simulating at them or extrapolating from pion masses, e.g. below 200 MeV to the physical pion mass value of 135 MeV) with controlled continuum extrapolation (at least three lattice spacings in the scaling region).

In this paper, full results from the Budapest–Marseille–Wuppertal Collaboration are summarized. We used both staggered and Wilson fermions (and for one illustrative purpose overlap fermions). Independently of the fermion formulation, the gauge action was a tree-level improved Symanzik gauge action [11–13]. In the fermion operator we always used stout smearing [14]. For the staggered case, two steps of smearing were applied (first seen in Ref. [15]). These lattices have been used almost exclusively for thermodynamics studies. At $T = 0$ we mostly used Wilson fermions with six stout smearings (recursively, as done for the first time in Ref. [16]) or constraining these smearing steps within a hypercube (HEX smearing, first used in our case in Ref. [17]).

The reason for this mixed setup (mostly Wilson fermions at $T = 0$, and almost always staggered fermions for thermodynamics) can be summarized as follows. Staggered fermions are numerically about an order of magnitude cheaper. They still have a remnant of the chiral symmetry of the continuum action. Wilson fermions are theoretically in some sense cleaner (no need for rooting). Though

speed and computational costs are always important, we decided to work at $T = 0$ with the theoretically cleaner Wilson fermions. Since it is possible to reach physical quark masses and/or lattice spacing down to about 0.05 fm with Wilson fermions, there is no need for further justification of this choice. It is clean and doable.

In thermodynamics, the basic process is the chiral phase transition (for vanishing quark masses) or the remnant of it (for physical quark masses). For this procedure, it is advantageous to have a staggered fermion formulation with remnant chiral symmetry. As a cross-check, we carried out the same study (transition from the hadron-dominated phase to the phase in which colored degrees of freedom are dominant) with Wilson fermions, too. As expected, it is much more CPU-demanding and the continuum limit can only be reached by using smaller lattice spacings than for the staggered case (even though here we could not yet reach the physical quark masses). In the long term it is necessary to repeat all these staggered studies with a theoretically clean lattice formulation. Clearly, experiments and phenomenological model building urgently need the results coming from lattice QCD. Thus, it is important to provide these results in a timely manner now, and carry out the calculations with formulations, which are completely free of theoretical concerns, later.

The paper is structured as follows. In Sect. 2, $T = 0$ physics is discussed. The advantage of smearing is illustrated. A fully controlled determination of the light hadron spectrum is presented. The light and strange quark masses are calculated. The kaon bag parameter is determined. In Sect. 3, QCD at nonvanishing temperatures is studied. The nature of the transition is analyzed. The transition temperature and the equation of state are calculated. Section 4 deals with nonvanishing chemical potentials and magnetic fields. Results for the phase diagram and equation of state are presented.

2. QCD at vanishing temperatures

This section of the report presents some selected $T = 0$ lattice QCD results of the Budapest–Marseille–Wuppertal Collaboration. The vast majority of our $T = 0$ results were obtained using smeared Wilson fermions. We utilized two types of very similar smearing. For the spectrum calculation and for F_K/F_π, we applied six steps of stout smearing at three lattice spacings down to 0.065 fm and pion masses down to 190 MeV (we call this our 2008 data set). For the quark mass determination and for the B_K analysis, two steps of HEX smearing were applied. We call this our 2010 data set, which covers five lattice spacings down to 0.054 fm and pion masses down to 120 MeV. These pion masses enabled an interpolation to the physical mass point. In both data sets the strange quark mass was set to its approximate physical value.

2.1. Light hadron spectrum

This subsection summarizes our light hadron spectrum analysis [18] (for a recent review on the topic see Ref. [19]).

Let us briefly mention some previous works. Calculations have been performed using the quenched approximation, which assumes that the fermion determinant (obtained after integrating over the ψ fields) is independent of the gauge field. Although this approach omits the most computationally demanding part of a full QCD calculation, a thorough determination of the quenched spectrum took almost 20 years. It was shown [20] that the quenched theory agreed with the experimental spectrum to approximately 10% for typical hadron masses and demonstrated that systematic differences were observed between quenched and two flavor QCD beyond that level of precision [20,21].

Including the effects of the light sea quarks has dramatically improved the agreement between experiment and lattice QCD results. Five years ago, a collaboration of collaborations [22] produced results for many physical quantities that agreed well with experimental results. Thanks to continuous progress since then, lattice QCD calculations can now be performed with light sea quarks whose masses are very close to their physical values [23] (though in quite small volumes). Other calculations, which include these sea-quark effects in the light hadron spectrum, have also appeared in the literature [24–32].

We aimed at a full calculation controlling all the systematic uncertainties. To that end we set up five conditions (these conditions are accepted by a large fraction of the community as reliable; of course one can choose other conditions and can focus on other points of interest). These conditions are listed below and a few of them are briefly commented on in parenthesis concerning our analysis.

I. The inclusion of the up (u), down (d), and strange (s) quarks in the fermion determinant with an exact algorithm and with an action whose universality class is QCD. For the light hadron spectrum, the effects of the heavier charm, bottom, and top quarks are included in the coupling constant and light quark masses.

II. A complete determination of the masses of the light ground-state, flavor nonsinglet mesons and octet and decuplet baryons. Three of these are used to fix the masses of the isospin averaged light (m_{ud}) and strange (m_s) quark masses and the overall scale in physical units. (We set the overall scale by using the two most precise hadron masses of our analysis: in one case it was the Ξ, in the other case it was the Ω baryon.)

III. Large volumes to guarantee small finite-size effects and at least one data point at a significantly larger volume to confirm the smallness of these effects. In large volumes, finite-size corrections to the spectrum are exponentially small [33,34]. As a conservative rule of thumb, $M_\pi L \gtrsim 4$, with M_π the pion mass and L the lattice size, guarantees that finite-volume errors in the spectrum are around or below the percent level. Resonances require special care. Their finite volume behavior is more involved. The literature provides a conceptually satisfactory framework for these effects [35,36], which should be included in the analysis. (For one of our simulation points we used several volumes and determined the volume dependence, which was in good agreement with Ref. [37]. This was included as a negligible correction at all points. We also calculated the corrections necessary to reconstruct the resonance masses from the finite volume ground-state energy and included them.)

IV. Controlled interpolations and extrapolations of the results to physical m_{ud} and m_s (or eventually directly simulating at these mass values). Although interpolations to physical m_s, corresponding to $M_K \simeq 495$ MeV, are straightforward, the extrapolations to the physical value of m_{ud}, corresponding to $M_\pi \simeq 135$ MeV, are difficult. They need computationally intensive calculations with M_π reaching down to 200 MeV or less. (We used chiral perturbation theory and Taylor expansion to reach the physical value of the pion mass from our 190 MeV pion mass point.)

V. Controlled extrapolations to the continuum limit, requiring that the calculations be performed at no less than three values of the lattice spacing, in order to guarantee that the scaling region is reached. (Our three-flavor scaling study [16] showed that hadron masses deviate from their continuum values by less than approximately 1% for lattice spacings up to $a \approx 0.125$ fm. This observation was confirmed by the present analysis.)

Our analysis includes all five ingredients listed above. The combined extrapolation to the physical mass point and to the continuum limit is shown in Fig. 1.

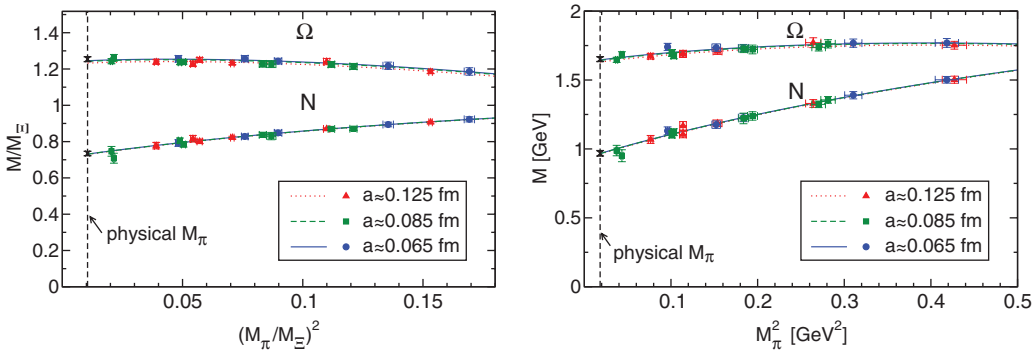

Fig. 1. Pion mass dependence of the nucleon (N) and Ω for all three values of the lattice spacing. Left panel: masses normalized by M_Ξ, evaluated at the corresponding simulation points. Right panel: masses in physical units. The scale in this case is set by M_Ξ at the physical point. Triangles on dotted lines correspond to $a \approx 0.125$ fm, squares on dashed lines to $a \approx 0.085$ fm, and circles on solid lines to $a \approx 0.065$ fm. The points were obtained by interpolating the lattice results to the physical m_s (defined by setting $2M_K^2 - M_\pi^2$ to its physical value). The curves are the corresponding fits. The crosses are the continuum extrapolated values in the physical pion mass limit. The lattice-spacing dependence of the results is barely significant statistically, despite the factor of 3.7 separating the squares of the largest ($a \approx 0.125$ fm) and smallest ($a \approx 0.065$ fm) lattice spacings. The χ^2/degrees of freedom values of the fits in the left panel are 9.46/14 (Ω) and 7.10/14 (N), whereas those of the fits in the right panel are 10.6/14 (Ω) and 9.33/14 (N), respectively.

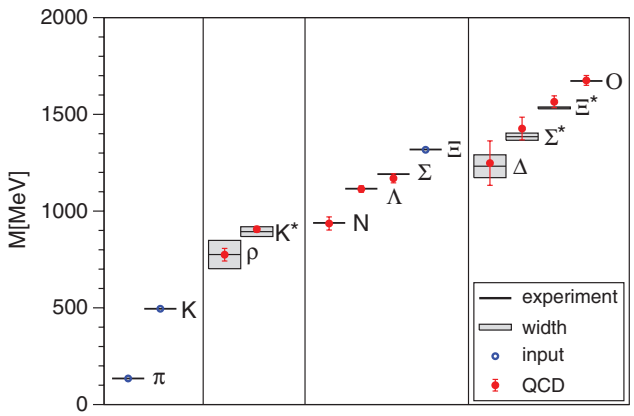

Fig. 2. The light hadron spectrum of QCD. Horizontal lines and bands are the experimental values with their decay widths. Our results are shown by solid circles. Vertical error bars represent our combined statistical and systematic error estimates. π, K, and Ξ have no error bars, because they are used to set the light quark mass, the strange quark mass, and the overall scale, respectively.

As already mentioned, we performed two separate analyses, setting the scale with M_Ξ and M_Ω. The results of these two sets are in perfect agreement. The Ξ set is shown in Fig. 2. With both scale-setting procedures we find that the masses agree with the hadron spectrum observed in nature [38].

2.2. *The ratio of F_K/F_π*

We used the same 2008 data set (which was used to determine the light hadron spectrum) to determine F_K/F_π in the physical limit (extrapolated to physical quark masses and into the continuum limit). The details of the calculation can be found in Ref. [39].

In that paper we followed a proposal by Marciano [40] to derive $|V_{us}|$ from $|V_{ud}|$, using a lattice determination of the ratio F_K/F_π of leptonic decay constants. More specifically, in

$$\frac{\Gamma(K \to l\bar{\nu}_l)}{\Gamma(\pi \to l\bar{\nu}_l)} = \frac{|V_{us}|^2}{|V_{ud}|^2}\frac{F_K^2}{F_\pi^2}\frac{M_K(1-m_l^2/M_K^2)^2}{M_\pi(1-m_l^2/M_\pi^2)^2}\left\{1+\frac{\alpha}{\pi}(C_K - C_\pi)\right\}, \tag{2.1}$$

the l.h.s. is known to 0.4% precision, even after dividing it by the radiative correction factor (the last bracket on the r.h.s.), if $l = \mu$ is considered [41]. Also, M_K, M_π, and m_μ are known with a relative precision of $3 \cdot 10^{-5}$, $3 \cdot 10^{-6}$, and 10^{-7}, respectively [41]. Additionally, $|V_{ud}|$ has been determined from super-allowed nuclear β-decays with an accuracy better than 0.03% [41,42]. Therefore, the limiting factor for a precise determination of $|V_{us}|$ via (2.1) is F_K/F_π—this ratio is typically determined with a precision of a few percent in present-day lattice QCD studies. Note that in this ratio the renormalization factors drop out, and thus one needs only the kaon and pion correlators and another quantity to set the scale.

We have presented a state-of-the art determination of F_K/F_π in QCD in which all sources of systematic uncertainty were properly taken into account. The central part of the analysis was to extrapolate to the physical point. In order to assess the theoretical error that arises in this extrapolation, we choose to invoke three frameworks to parametrize the quark mass dependence:

(*i*) SU(3) chiral perturbation theory (χPT) [43],
(*ii*) heavy kaon SU(2) chiral perturbation theory [44],
(*iii*) "Taylor" extrapolations involving polynomial ansaetze [45].

The following discussion illustrates our strategy to estimate systematic errors. Our results for F_K/F_π display a small dependence on lattice spacing. To estimate the systematic error associated with the continuum extrapolation, we consider fits with and without $O(a^2)$ and $O(a)$ Symanzik factors. These choices, with seven choices for the fitting strategies to the physical mass point, 18 different fitting intervals for the individual correlators, two scale-setting procedures, and two cuts for the pion mass range (350 and 460 MeV) provided us with $3 \times 7 \times 18 \times 2 \times 2 = 1512$ alternative analyses. The central value obtained from each procedure is weighted with the quality of the (correlated) fit to construct a distribution. The median and the 16th/84th percentiles yield the final central value and the systematic error associated with possible excited state contributions, scale setting, and the chiral and continuum extrapolations. To determine the statistical error, the whole procedure is bootstrapped (with 2000 samples) and the variance of the resulting medians is computed.

A "snapshot" fit (with a specific choice for the time intervals used in fitting the correlators, scale setting, and pion mass range) can be seen in Fig. 3. To avoid the complications of a multi-dimensional plot, the extrapolation is shown as a function of the pion mass only. The data have been corrected for the deviation of the simulated m_s from $m_s^{\rm phys}$.

Following the procedure outlined above, our final result is

$$\left.\frac{F_K}{F_\pi}\right|_{\rm phys} = 1.192(7)_{\rm stat}(6)_{\rm syst} \quad \text{or} \quad \left.\frac{F_\pi}{F_K}\right|_{\rm phys} = 0.839(5)_{\rm stat}(4)_{\rm syst} \tag{2.2}$$

at the physical point.

With the result (2.2) in hand, we can now focus on Cabibbo-Kobayashi-Maskawa (CKM) matrix elements. In this respect there are two options: we may *assume* the standard model (and hence CKM unitarity) and determine $|V_{ud}|$ and $|V_{us}|$, or we may use phenomenological input on $|V_{ud}|$ to derive $|V_{us}|$ and hence *test* CKM unitarity (under the assumption of quark-flavor universality) in a model-independent way.

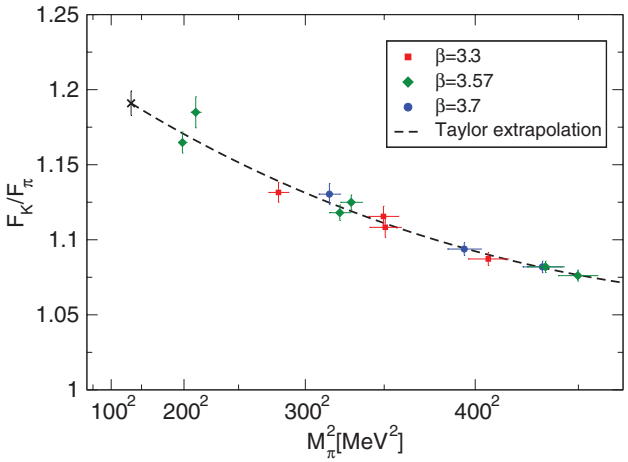

Fig. 3. Extrapolation of the lattice data to the physical point for a particular choice of two-point function fits ($t_{\min}/a = 6, 8, 11$ for $\beta = 3.3, 3.57, 3.7$, respectively), mass cut ($M_\pi < 460\,\text{MeV}$), and using the Ξ to set the scale. The plot shows one (of the 21) fits used to estimate the uncertainty associated with the functional form used for the mass extrapolation. The data have been slightly adjusted to the physical strange quark mass, as well as corrected for tiny finite-volume effects (see text for details).

The first step, needed in either case, is to simplify Marciano's equation. The Flavianet kaon working group gave [46]

$$\frac{|V_{us}|}{|V_{ud}|}\frac{F_K}{F_\pi} = 0.275\,99(59). \tag{2.3}$$

Combining this with our result (2.2) yields the ratio

$$|V_{us}|/|V_{ud}| = 0.2315(19). \tag{2.4}$$

Now for the two options. If we assume unitarity, (2.4) and Ref. [41] $|V_{ub}| = (3.93 \pm 0.36) \cdot 10^{-3}$ imply

$$|V_{ud}| = 0.97422(40), \quad |V_{us}| = 0.2256(17). \tag{2.5}$$

On the other hand, if we combine (2.4) with the most precise information on the first CKM matrix element available today, $|V_{ud}| = 0.974\,25(22)$ [42], we obtain (again)

$$|V_{us}| = 0.2256(18). \tag{2.6}$$

Similarly, by also including the above-mentioned result for $|V_{ub}|$, we find

$$|V_{ud}|^2 + |V_{us}|^2 + |V_{ub}|^2 = 1.0001(9). \tag{2.7}$$

With the first-row unitarity relation (which is genuine to the CKM paradigm) being so well observed, there is no support for "beyond the standard model" physics contributions to these processes.

2.3. Light and strange quark masses

Interestingly enough, the experimental data for m_u, m_d, and m_s have been available for about sixty years (the pion and kaon were discovered in the late 1940s and the proton 30 years before). Even the theory of the strong interaction, QCD, which—in principle—completely describes bound states of light quarks, has been known for almost four decades [47]. The fact that such a fundamental question has remained poorly answered despite the available experimental and theoretical knowledge is related to the computational difficulties one encounters when trying to solve the underlying equations in

the domain of interest. The only known systematic technique to solve them is lattice QCD [1,48]. Several decades of theoretical, algorithmic, and hardware development have been necessary to reach the level at which the light quark masses can be determined reliably. This determination is the goal of the present subsection.

For many years calculations were done in the quenched approximation. Although this approach omits the most computationally demanding part of a full QCD calculation—the quark determinant obtained after integrating over the fermion fields—a controlled determination of the strange quark mass in this approximation (with $m_u = m_d = m_s$ equal to about half the physical m_s) took about 20 years [49]. Moreover, the physics of the u and d quarks remained inaccessible, because the quenched approximation, an uncontrolled truncation of QCD, distorts the small quark mass behavior [50,51].

A very important step in the determination of light quark masses was made with the inclusion of u and d sea quark effects ($N_f = 2$) [52–56]. But even there, the physical m_{ud} remained elusive, this time for algorithmic reasons. A first breakthrough was made by the MILC Collaboration [57], which used an $N_f = 2 + 1$ staggered fermion formulation to include strange sea quark effects, pushing calculations to smaller light quark masses, finer lattices, and larger volumes. Updates from calculations with sea pion masses down to 258 MeV (given by the RMS average over taste partners for $a = 0.06$ fm—their lightest valence pion is 177 MeV at $a = 0.09$ fm) [58] and on even finer lattices are presented in Refs. [58,59]. On a subset of the MILC configurations, the HPQCD Collaboration has obtained m_s and m_{ud} indirectly via the m_c/m_s ratio [60,61]. Recently, ETMC ($N_f = 2$) [62] and RBC-UKQCD ($N_f = 2 + 1$) [63] have also presented results with $M_\pi \gtrsim 270$ MeV and significantly larger error bars. All $N_f = 2 + 1$ results for m_s and m_{ud} (except for those of the very recent Ref. [63]) were combined into world averages in Ref. [64], which also reviews $N_f = 2$ and nonlattice results. Our results are in complete agreement with these averages.

In the two previous subsections two illustrative works were presented, which used our 2008 data set. The present (and also the next) subsection deals with the 2010 data set. This data set contains five lattice spacings ($a \approx 0.116, 0.093, 0.077, 0.065$, and 0.054 fm), which are the basis for the continuum extrapolation. As we observed, the difference between the results obtained on the finest lattice and those in the continuum limit was $\sim 3\%$, whereas that between those of the coarsest lattice and the continuum limit was $\sim$10%. Our data set contains physical or smaller than physical quark masses for three of the lattice spacings. The data set is well illustrated on a plot showing the pion mass and the spatial extension (Fig. 4). The details of the quark mass determination can be found in Refs. [17,65].

In the present analysis (determination of the light and strange quark masses) essentially the same conditions should be applied as for the case of the light hadron spectrum. In addition to the hadron masses, the unrenormalized partially conserved axial current (PCAC) quark masses are determined.

Since the quark masses depend on the renormalization scheme, we need in addition a fully nonperturbative renormalization procedure. In addition to the PCAC masses discussed above, the bare m_{ud} and m_s in the Lagrangian also provide a measure of the quark masses used in our simulations. Once suitably renormalized, these two definitions yield quark masses that must agree in the continuum limit.

While the PCAC masses renormalize multiplicatively, the bare Lagrangian masses require an additional additive renormalization. In the difference $d \equiv m_s^{\rm bare} - m_{ud}^{\rm bare}$, this additive renormalization is eliminated. Moreover, the multiplicative renormalization factors cancel in the ratio $r \equiv m_s^{\rm PCAC}/m_{ud}^{\rm PCAC}$. To obtain fully renormalized quantities, we must still multiply d by $1/Z_S$, the inverse of the scalar density renormalization factor. From the renormalized mass difference d/Z_S and the renormalization independent ratio r we obtain $m_{ud}^{\rm ren} = (d/Z_S)/(r-1)$ and $m_s^{\rm ren} = (rd/Z_S)/(r-1)$

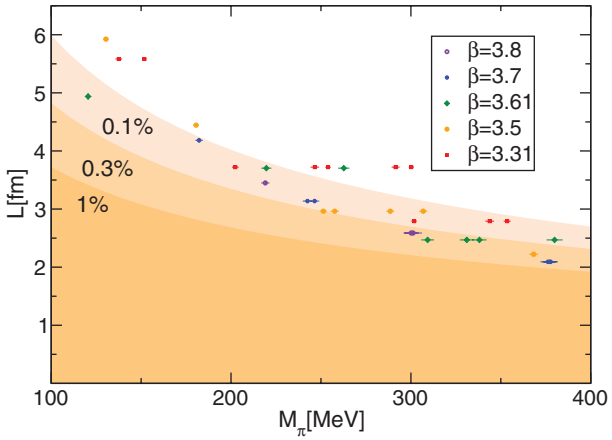

Fig. 4. Summary of our simulation points. The pion masses and the spatial sizes of the lattices are shown for our five lattice spacings. The percentage labels indicate regions, in which the expected finite volume effect [37] on M_π is larger than 1%, 0.3%, and 0.1%, respectively. This effect is smaller than about 0.5% for all of our runs and, as described, we corrected for it. Error bars are statistical.

in the unimproved case. Our final analysis is tree-level $\mathcal{O}(a)$ improved with slightly more complicated formulae (see Sect. 11.2 of Ref. [17]).

The strange and average up-down quark masses renormalized in the regularization independent (RI) scheme at 4 GeV are extrapolated to the continuum and interpolated to the physical mass point. In these fits, we include terms to correct linear ($\alpha_s a$) or quadratic (a^2) cutoff effects. A combined mass and lattice spacing fit is carried out. We show the continuum extrapolation for m_{ud} and m_s in the RI scheme at 4 GeV, as well as their ratio, in Fig. 5. In order to control the systematic uncertainties we carry out 288 such analyses [17]. The figure depicts results from one analysis with one of the best fit qualities.

The determination of the individual up and down quark masses at the physical point is in principle possible using exclusively lattice simulations. To that end one may include the electromagnetic U(1) gauge field in the lattice framework, as was done recently in Ref. [66]. We have not carried out such a calculation (yet). Nevertheless, our precise m_s and m_{ud} values can be combined [17] with model-independent results based on dispersive studies of $\eta \to 3\pi$ decays to derive the individual up and down quark masses (see Table 1). In this approach the relationship between the input parameters and experiments is not as transparent as for the determination of m_s and m_{ud} (for details see Ref. [17]).

2.4. Precision computation of the kaon bag parameter

Another quantity that we determined with our 2010 data set was the kaon bag parameter, B_K.

Neutral kaon mixing is responsible for indirect CP-violation in $K \to \pi\pi$ decays. This violation is quantified by the parameter ϵ, which is related to quark flavor mixing parameters and the ratio of hadronic matrix elements

$$B_K = \frac{\langle \bar{K}^0 | O^{\Delta S=2} | K^0 \rangle}{\frac{8}{3} \langle \bar{K}^0 | A_\mu | 0 \rangle \langle 0 | A^\mu | K^0 \rangle}, \tag{2.8}$$

where $O^{\Delta S=2} = [\bar{s}\gamma_\mu(1-\gamma_5)d][\bar{s}\gamma^\mu(1-\gamma_5)d]$ (see Ref. [64] for details). One particular point to note is that our lattice discretized fermion action only exhibits approximate chiral symmetry that gets fully restored in the continuum limit only. Consequently, mixing of the standard model operator, which has the structure $O_1 = (V-A)(V-A)$, with other dimension-6 operators is allowed at finite

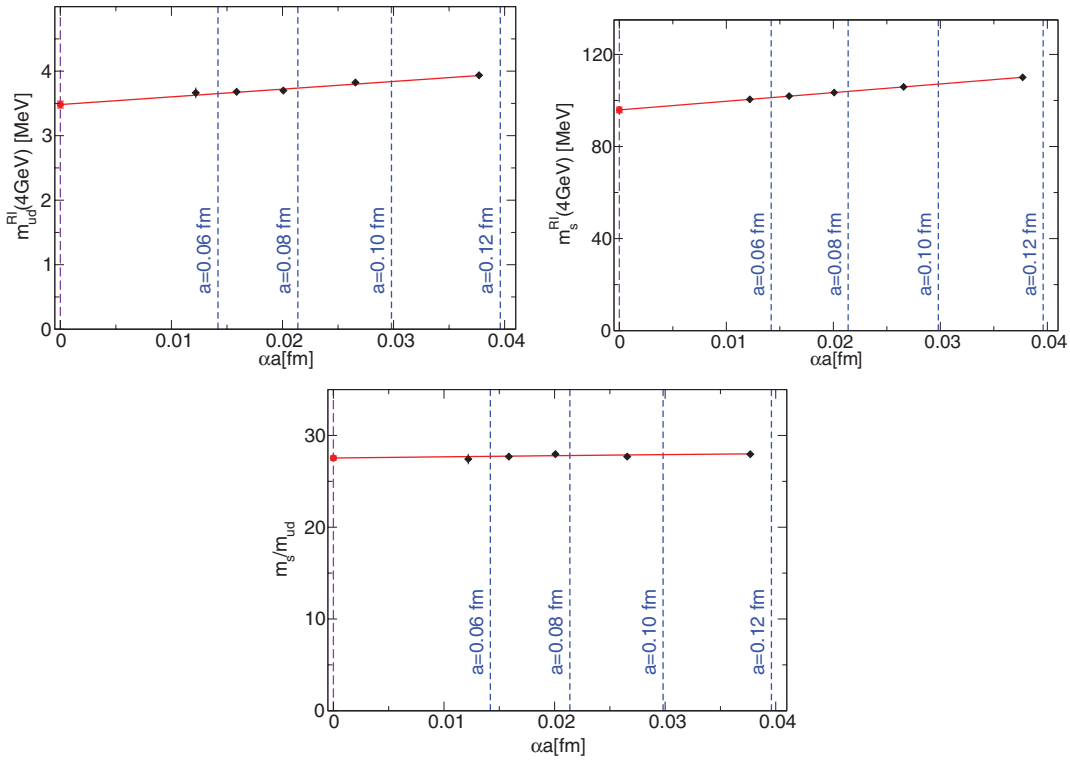

Fig. 5. Continuum extrapolation of the average up/down quark mass, of the strange quark mass, and of the ratio of the two. The errors of the individual points, which are statistical only here, are smaller than the symbols in most of the cases. The only exceptions are the light quark mass and its ratio to the strange quark mass at the two finest lattice spacings. These exceptions underline the importance of using physical quark masses to reach a high accuracy.

Table 1. Renormalized quark masses in the RI scheme at 4 GeV, and after conversion to RGI and the $\overline{MS}$ scheme at 2 GeV. The RI values are fully nonperturbative, so the first column is our main result. The first two rows emerge directly from our lattice calculation. The last two include additional dispersive information.

	RI (4 GeV)	RGI	$\overline{MS}$ (2 GeV)
m_s	96.4(1.1)(1.5)	127.3(1.5)(1.9)	95.5(1.1)(1.5)
m_{ud}	3.503(48)(49)	4.624(63)(64)	3.469(47)(48)
m_u	2.17(04)(10)	2.86(05)(13)	2.15(03)(10)
m_d	4.84(07)(12)	6.39(09)(15)	4.79(07)(12)

lattice spacing, although it is forbidden in the continuum. These other operators are $O_2 = VV - AA$, $O_{3/4} = SS \mp PP$, and $O_5 = TT$. As the standard model operator is chirally suppressed, these mixings can in principle be very large. Due to the good approximate chiral symmetry of our action, [67] the mixing contributions to B_K are actually tiny, as displayed in Fig. 6.

Out of the five available lattice spacings, we use the four finest covering a range of 0.054 fm to 0.093 fm (the low momentum cutoff at the largest lattice spacing $a \approx 0.116$ fm does not allow for a reliable extraction of the mixing coefficients). The $N_f = 3$ configurations are used to compute the required renormalization constants nonperturbatively using the regularization independent momentum subtraction scheme method [68,69]. For each lattice spacing, we interpolate the renormalized

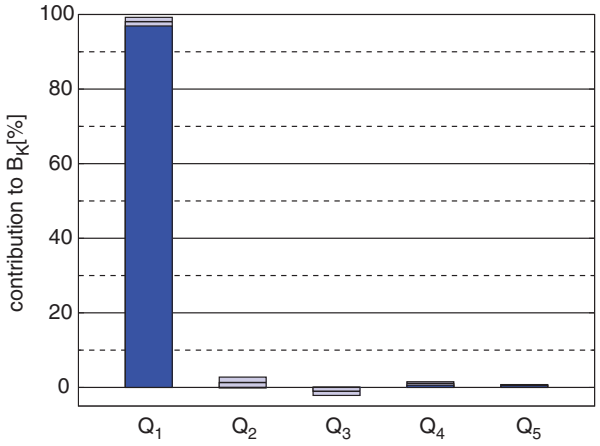

Fig. 6. Contribution of the various operators towards the final value of B_K for the ensemble with the lightest pion mass. The contribution from the standard model operator O_1 is clearly dominant.

B_K to physical pion and kaon masses using various interpolators, and the resulting physical value is extrapolated to the continuum.

Both interpolation to physical pion and kaon masses as well as the continuum extrapolation turn out to be very mild. In addition, the effect of finite volume corrections is even smaller than it was on quark masses. Consequently, the systematic error of our result is less than half the statistical error and we obtain

$$B_K^{\mathrm{RI-MOM}}(3.5\,\mathrm{GeV}) = 0.5308(56)(23) \tag{2.9}$$

as our final, fully nonperturbative result.

For further conversion of (2.9) into other schemes, we use results for the 2-loop running [70,71]. Adding a conservative perturbative conversion uncertainty of 1%, we obtain

$$B_K^{\overline{\mathrm{MS}}-\mathrm{NDR}}(2\,\mathrm{GeV}) = 0.5644(59)_{\mathrm{stat}}(25)_{\mathrm{sys}}(56)_{\mathrm{PT}} \tag{2.10}$$

$$\hat{B}_K = 0.7727(81)_{\mathrm{stat}}(34)_{\mathrm{sys}}(77)_{\mathrm{PT}} \tag{2.11}$$

The latter (renormalization group invariant (RGI) value) is compatible with the prediction $\hat{B}_K = 0.83^{+0.21}_{-0.15}$ from a global CKM fit [72].

3. QCD at nonvanishing temperatures

When we analyze the absolute scale or any other question related to the $T > 0$ QCD transition for the physically relevant case, two ingredients are quite important.

First of all, one should use physical quark masses. The nature of the transition strongly depends on the quark mass. Lattice studies and effective models showed that in the three flavor theory for small or large quark masses the transition is a first order phase transition, whereas for intermediate quark masses it is an analytic crossover (see later). Since the nature of the transition influences the absolute scale (transition temperature, T_c) of the transition—its value, mass dependence, uniqueness, etc.—the use of physical quark masses is also essential for the determination of T_c, too. The absolute scale then goes into all observables. While it is relatively easy to reach the physical value of the strange quark mass (m_s) in present-day lattice simulations, it is much more difficult to work with physical up and down (or, in other word, light) quark masses (m_{ud}), because they are much smaller: $m_s/m_{ud} \approx 28$. In calculations with m_s/m_{ud} smaller than 28 the strange quark mass is usually tuned

to its approximate physical value, whereas the average up and down quark masses are larger than the physical value.

Secondly, the nature and other characteristics of the $T > 0$ QCD transition is known to suffer from discretization errors [73,74]. Let us mention one example that underlines the importance of removing these discretization effects by performing a controlled continuum extrapolation. The three flavor theory with a large, $a \approx 0.3$ fm lattice spacing and standard staggered action predicts a critical pseudoscalar mass of about 300 MeV [75]. This point separates the first order and crossover regions. If we took another discretization, with another discretization error, the critical pseudoscalar mass turns out to be much smaller, well below the physical pion mass of 135 MeV. The only way to determine the physical features of the transition is to carry out a careful continuum limit analysis. This can be safely done only in the so-called scaling regime. This regime is reached when the lattice spacing (a) is sufficiently small, smaller than some $a_{\max}$. Dimensionless combinations of observables (within their error bars) approach their continuum limit value in the scaling regime with a correction term $c \cdot a^n$. Here c, n, and $a_{\max}$ (the lattice spacing from which the scaling regime starts) depend on the action and on the dimensionless combination. The values of c and $a_{\max}$ are typically unknown, whereas the form of the action and the observables provide the value for n, usually without performing any simulations. To carry out a controlled continuum extrapolation, at least three lattice spacings in the scaling regime are needed (two points will always lie on a two parameter $c \cdot a^n$ curve, independently of whether the lattice spacings are smaller than $a_{\max}$ or not; the third point indicates if one has reached the scaling regime).

It is numerically very demanding to fulfill both conditions. There are only a few cases for which this has been achieved. It is important to note that fulfilling the second condition without fulfilling the first one still leads to universal results. In other words, continuum extrapolated results with nonphysical quark masses are universal. Independently of the action, simulation algorithm, and scale setting procedure, they provide the same answer once the quark mass is fixed (which is a nontrivial issue, but can be done, e.g., by fixing the pion to rho and kaon to Omega mass ratios: M_π/M_ρ and M_K/M_Ω are fixed). These results are not the same as they are for physical quark masses, but they are well defined and unique. In contrast to this universality, fulfilling the first condition (physical quark mass) but not the second one leads to nonuniversal, nonphysical results. These results still have unknown discretization errors.

Once the available computational resources are insufficient to fulfill both conditions it is more advisable to carry out calculations with nonphysical quark masses but perform the continuum limit extrapolation. As we have seen, such results are universal and can be cross-checked with other results obtained by other fermion formalisms, actions etc.

In this section, QCD at nonvanishing temperatures is studied. We use three different actions: with staggered, Wilson, and overlap fermions. Most of the work of our collaboration (we usually use the name Wuppertal–Budapest Collaboration, though in the literature Budapest–Marseille–Wuppertal Collaboration is also used; note that with our colleagues in Marseille we usually carry out studies at $T = 0$) has been done with staggered fermions. In these studies, we used a Symanzik improved gauge and stout improved fermionic action [15]. The nature of the transition is determined (first order, second order, or analytic crossover). The absolute scale of the transition (T_c) was a controversial issue in the literature for many years. Now the disagreement is resolved and final results are presented. The equation of state is determined, for which various groups still have quite different results. The Wilson formalism was used to give continuum results for a larger than physical pion mass and the overlap framework was used as an exploratory study. All of them will be discussed here.

3.1. Nature of the QCD transition

As we will see, the nature of the transition is a crossover. This is a highly nontrivial result obtained with physical quark masses extrapolated to the continuum limit by performing a finite volume analysis. This result affects our understanding of the universe's evolution (see, e.g., Ref. [76]). In a strong first order phase transition scenario the quark–gluon plasma super-cools before bubbles of hadron gas are formed. These bubbles grow, collide, and merge, during which gravitational waves could be produced [77]. Baryon enriched nuggets could remain between the bubbles contributing to dark matter. Since the hadronic phase is the initial condition for nucleosynthesis, the above picture with inhomogeneities could have a strong effect on it [78]. As the first order phase transition weakens, these effects become less pronounced. Recent calculations provide strong evidence that the QCD transition is an analytic transition (what we call here a crossover), and thus the above scenarios—and many others—are ruled out.

In order to determine the nature of the transition one should apply finite size scaling techniques for the chiral susceptibility [79]. The most straightforward way is to look at the second derivative of the partition function Z with respect to the light quark masses m_{ud} at a temperature T and volume V. One obtains $\chi = (T/V) \cdot (\partial^2 \log Z/\partial m_{ud}^2)$. This quantity shows a pronounced peak as a function of the temperature. For a first order phase transition, such as in the pure gauge theory, the peak of the analogous Polyakov susceptibility gets more and more singular as we increase the volume. A second order transition shows a similar singular behavior with critical indices. For an analytic transition (crossover) the peak width and height saturate to a constant value.

One can carry out a finite size scaling analysis with the continuum extrapolated height of the renormalized susceptibility. The renormalization of the chiral susceptibility can be done by taking the second derivative of the free energy density (f) with respect to the renormalized mass (m_r). The logarithm of the partition function contains quartic divergences. These can be removed by subtracting the free energy at $T = 0$: $f/T^4 = -N_t^4 \cdot [\log Z(N_s, N_t)/(N_t N_s^3) - \log Z(N_{s0}, N_{t0})/(N_{t0} N_{s0}^3)]$. This quantity has a correct continuum limit. The subtraction term is obtained at $T = 0$, for which simulations are carried out on lattices with N_{s0}, N_{t0} spatial and temporal extensions (otherwise at the same parameters of the action). The bare light quark mass (m_{ud}) is related to m_r by the mass renormalization constant $m_r = Z_m \cdot m_{ud}$. Note that Z_m falls out of the combination $m_r^2 \partial^2/\partial m_r^2 = m_{ud}^2 \partial^2/\partial m_{ud}^2$. Thus, $m_{ud}^2[\chi(N_s, N_t) - \chi(N_{s0}, N_{t0})]$ also has a continuum limit (for its maximum values for different N_t, and in the continuum limit we use the shorthand notation $m^2 \Delta\chi$).

In order to carry out the finite volume scaling in the continuum limit, three different physical volumes were taken. For these volumes the dimensionless combination $T^4/(m^2 \Delta\chi)$ was calculated at 4 different lattice spacings. The volume dependence of the continuum extrapolated inverse susceptibilities is shown in Fig. 7.

The result is consistent with an approximately constant behavior, despite the fact that there was a factor of 5 difference in the volume. The chance probabilities that statistical fluctuations changed the dominant behavior of the volume dependence are negligible. As a conclusion we can saythat the staggered QCD transition at $\mu = 0$ is a crossover.

An analytic crossover, like the QCD transition, has no unique T_c. A particularly nice example of this is the water–vapor transition (see Fig. 8). Up to about 650 K the transition is a first order one, which ends at a second order critical point. For a first or second order phase transition the different observables (such as density or heat capacity) have their singularity (a jump or an infinitely high peak) at the same pressure. However, at even higher temperatures the transition is an analytic crossover,

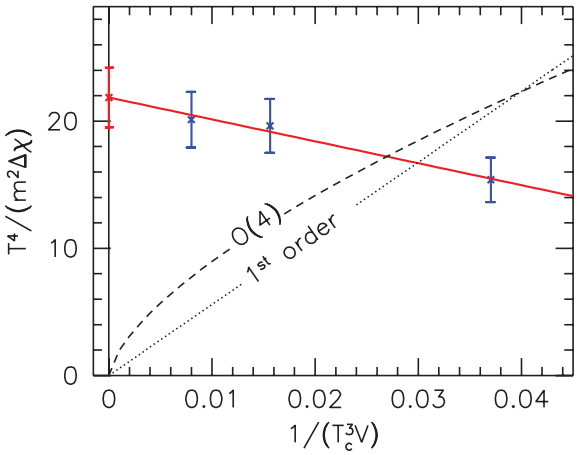

Fig. 7. Continuum extrapolated susceptibilities $T^4/(m^2\Delta\chi)$ as a function of $1/(T_c^3 V)$. For true phase transitions the infinite volume extrapolation should be consistent with zero, whereas for an analytic crossover the infinite volume extrapolation gives a nonvanishing value. The continuum-extrapolated susceptibilities show no phase-transition-like volume dependence, though the volume changes by a factor of five. The $V \to \infty$ extrapolated value is 22(2), which is 11σ away from zero. For illustration, we fit the expected asymptotic behavior for first-order and O(4) (second-order) phase transitions, shown by dotted and dashed lines, which results in chance probabilities of 10^{-19} (7×10^{-13}), respectively.

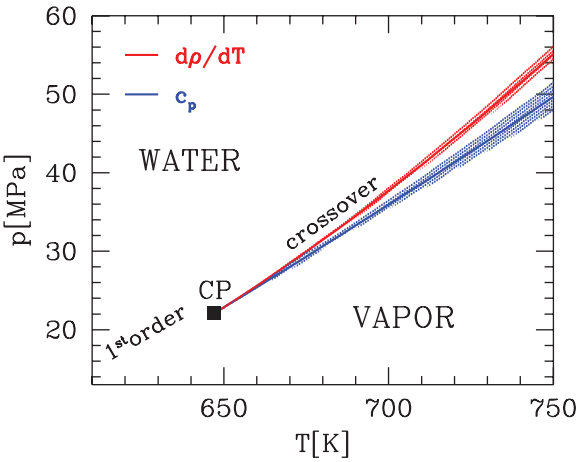

Fig. 8. The water–vapor phase diagram.

for which the most singular points are different. The blue curve shows the peak of the heat capacity and the red one the inflection point of the density. Clearly, these transition temperatures are different, which is a characteristic feature of an analytic transition (crossover).

3.2. Transition temperature

One of the most interesting quantities that can be extracted from lattice simulations is the transition temperature T_c at which hadronic matter is supposed to undergo a transition to a deconfined, quark–gluon phase. This quantity has been vastly debated over the last few years, due to the disagreement on its numerical value observed by different lattice collaborations, which in some cases was as high as 20% of the absolute value. Indeed, the analysis of the Bielefeld–Brookhaven–Columbia–Riken Collaboration and later that of the hotQCD Collaboration (performed first with p4 and later

with two different improved staggered fermion actions, asqtad and p4, and with a physical strange quark mass and somewhat larger than physical u and d quark masses, $m_s/m_{u,d} = 10$) indicated that the transition region was in the range $T = (185 - 195)$ MeV. Different observables led to the same value of T_c [80–83]. Later, simulations using the p4 action with the quark mass ratio $m_s/m_u = 20$ yielded about 5 MeV shift (towards the smaller values) in the temperature dependence of the studied observables [84].

These results were in contradiction with our findings. We used the staggered stout action (with physical light and strange quark masses, thus $m_s/m_{u,d} \simeq 28$) and the value of the transition temperature was in the range 150–170 MeV, and it changes with the observable used to define it [85–87]. This is not surprising, since the transition is a crossover [79]: in this case it is possible to speak about a transition region, in which different observables may have their characteristic points at different temperature values, and the temperature dependences of the various observables play a more important role than any single T_c value. Unfortunately, the discrepancy was observed between the two collaborations for the T dependences of the various observables, too (thus, not only for their characteristic points, such as peak position or inflection point). All in all there was a discrepancy of about 40 MeV for quantities that monitored the remnant of the chiral phase transition and about 20 MeV for other quantities, e.g. the strange quark number susceptibility.

In our three papers dealing with the transition temperatures, [85–87] we presented a full analysis. There were three main ingredients of the analysis. 1. We used physical values of the quark masses both at $T = 0$ and $T > 0$ (in Ref. [85] chiral extrapolations were also performed at vanishing temperatures). 2. Furthermore, in order to verify that our results were independent of the physical quantity we chose to set the scale, we measured five experimentally well-known quantities. 3. In addition, we extended our finite temperature simulations by taking smaller and smaller lattice spacings (up to $N_t = 10$ in Ref. [85], up to $N_t = 12$ in Ref. [86], and up to $N_t = 16$ in Ref. [87].

ad 1. The easiest technique to avoid uncertainties related to chiral extrapolations is to work with physical quark masses (a better expression for the "chiral extrapolation" is actually "extrapolation to physical quark masses"; nevertheless, the wording "chiral extrapolation" is often used, since the up and down quark masses are so small—a few MeV—that they are almost zero compared to the typical hadronic scales, which have an order of magnitude of a GeV). This is obviously expensive; however, with our action it was possible even in 2005 to work with physical quark masses. To this end we extensively used graphic cards, first programming them in Cg and OpenGL [88], and later in CUDA. We have determined the lines of constant physics (LCP) and the scale using three quantities: kaon and pion mass and the kaon decay constant. We look for those strange and light quark mass parameters where M_π/f_K and M_K/f_K take their experimental values exactly. Taking f_K as a scale setting parameter turned out to be advantageous, most particularly since it can be measured more precisely and in a more unambiguous way than other scale setting parameters, e.g. r_0 or r_1.

ad 2. A necessary condition for the correctness of the finite temperature results is that zero temperature observables in the continuum limit are consistent with experiments. Moreover, the lattice spacing dependence of the zero temperature observables can give a hint on the lattice spacing range, where lattice artifacts are expected to scale as a^2.

Let us first take a look at various hadron masses (see left panel of Fig. 9). At the top of the figure the mass of the Ω baryon is plotted as a function of the lattice spacing squared. The red band is the experimental value of the Ω mass together with its uncertainty (to which the experimental uncertainty of our scale fixing quantity f_K also contributes). Our four finest lattice spacings are nicely consistent with the experiments. This fact confirms the correctness of the f_K-based scale setting procedure.

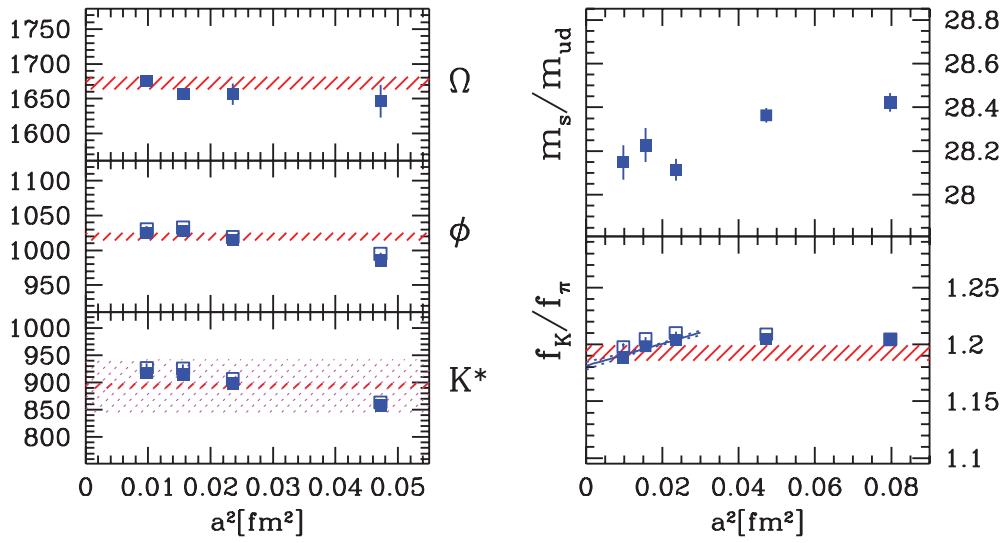

Fig. 9. Left panel: masses of the Ω baryon, $\phi(1020)$ meson, and $K^*(892)$ meson in MeV on our four finest lattices as a function of the lattice spacing squared. Right panel: quark mass ratio and f_K/f_π for all five ensembles. See text for a detailed explanation.

In other words, we have shown that performing the scale setting with the Ω mass would give the same continuum values for T_c in physical units.

The $\phi(1020)$ meson mass is plotted in the middle. The open and solid symbols correspond to two different vector meson operators (MIII and MIV using the notations of Ref. [89]); they are supposed to give the same mass in the continuum limit. We use only the connected part of the operators when evaluating the propagators (the disconnected part is very expensive to calculate; however, as large scale $T = 0$ simulations show [23], omitting the disconnected part for $\phi(1020)$ could provide the proper scale; the uncertainty related to this choice is subdominant). The plot also shows the agreement with experiment (red band).

The lower plot shows the $K^*(892)$ vector meson mass. Open and solid symbols are the two vector meson operators, as in the case of $\phi(1020)$. The agreement is somewhat worse than for the other two masses. However, one has to keep in mind that, at the physical point in our boxes, the strong decay of $K^*(892)$ is kinematically allowed. Our operators are supposed to have negligibly small coupling to scattering states and couple mostly to the resonance. The resonance energy level at a given volume is not necessarily the central value of the resonance (m_{K*}), but it might be some other value within the resonance distribution (which has Γ_{K*} width). Therefore, beside the red band, which is the experimental value of the $K^*(892)$ mass, we also draw a $2\Gamma_{K*}$ wide magenta band inside which the resonance levels are expected to appear (for a more complete treatment of the resonances see Ref. [18], a work that is briefly reviewed in the section on $T = 0$ physics).

The right panel of Fig. 9 shows the ratio of the strange and light quark masses. Note that this is not the ratio along the LCP (which was fixed to $m_s^{\rm LCP}/m_{ud}^{\rm LCP} = 27.3$), but the ratio of the quark masses after carrying out the correction to the LCP. As one can clearly see, there is no observable lattice spacing dependence for our three smallest lattice spacings. Therefore it is completely justified to take the result on the finest lattice spacing as the continuum estimate for the quark mass ratio: $m_s/m_{ud} = 28.15$. The statistical error is on the 0.4% level, the systematic uncertainties are somewhat larger.

In the lower part of the right panel we plot the ratio of kaon and pion decay constants against the lattice spacing squared for all five ensembles. The red band is the current best estimate for f_K/f_π including the uncertainty. Open symbols are the original lattice data, whereas solid ones contain the continuum limit finite volume corrections [90]. For the three finest lattice spacings we can observe a clear decreasing tendency. An extrapolation with an a^2 scaling function yields $f_K/f_\pi = 1.181$ in the continuum limit. The statistical error of f_K/f_π is on the 0.3% level. The systematic uncertainties are of the same order of magnitude.

The basic message of this analysis can be summarized as follows. Using an f_K based scale setting procedure, the masses of Ω, $K^*(892)$, $\phi(1020)$, and the pion decay constant are consistent with their experimental values on our finest lattices. This implies that, independently of which of these quantities is used for scale setting, we would obtain the same results in the continuum limit.

ad 3. As was emphasized, both groups extended the lattice spacings to smaller and smaller values. Several observables were determined and compared. Quark number susceptibilities are defined in the following way:

$$\chi_2^q = \frac{T}{V}\frac{\partial^2 \ln Z}{\partial(\mu_q)^2}\bigg|_{\mu_i=0}, \quad q = u, d, s. \tag{3.1}$$

These quantities rapidly increase during the transition, and therefore they can be used to identify this region.

The Polyakov loop is the order parameter related to the deconfinement phase transition of QCD in the pure gauge sector. In this case, the Z_3 symmetry is exact at small temperatures, where the Polyakov loop expectation value is zero. In the deconfined phase, this symmetry is spontaneously broken by the expectation value of the Polyakov loop, which jumps to a finite value. When quarks are included in the system, the Z_3 symmetry is explicitly broken by their presence. In this case, the Polyakov loop is no longer a real order parameter. Nevertheless, it is still considered as an indicator for the transition, since it exhibits a rise in the transition region. The need to renormalize it comes from the fact that there are self-energy contributions to the static quark free energy that need to be eliminated. To that end, we worked out a renormalization procedure [85]. In order to compare our results with those obtained by the hotQCD Collaboration [83], the renormalization constant is obtained slightly differently from the condition $V(1.5r_0) = V_{\rm string}(1.5r_0)$, where V is the zero temperature quark–antiquark potential and $V_{\rm string}(r) = -\pi/12r + \sigma r$. (Note that this definition of Ref. [87] is somewhat different from the ones we used in Refs. [85,86]; the reason for this change was merely the need to directly compare our results with those of the hotQCD Collaboration, who used this convention. The comparison for the Polyakov loop worked perfectly: the two collaborations obtained the same temperature dependence for this quantity.)

The chiral condensate is defined in the following way:

$$\langle\bar\psi\psi\rangle_q = \frac{T}{V}\frac{\partial \ln Z}{\partial m_q}, \quad q = u, d, s. \tag{3.2}$$

In the case of a real chiral phase transition, the chiral condensate is the corresponding order parameter. However, with physical quark masses there is no real phase transition, just a crossover. The chiral condensate can still be taken as an indicator for the remnant of the chiral transition, since it rapidly changes in the transition region.

In our papers, the following definition of the renormalized chiral condensate was used:

$$\langle\bar\psi\psi\rangle_R = -\left[\langle\bar\psi\psi\rangle_{l,T} - \langle\bar\psi\psi\rangle_{l,0}\right]\frac{m_l}{X^4} \quad l = u, d. \tag{3.3}$$

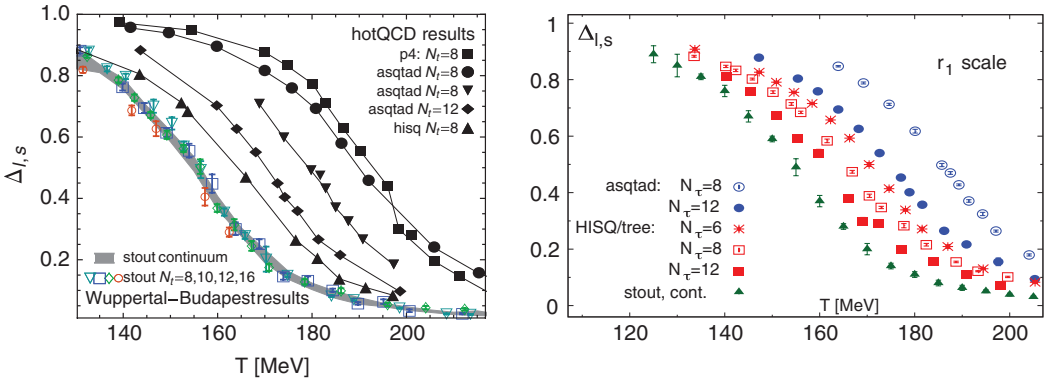

Fig. 10. Comparison of the strange subtracted chiral condensate for the Wuppertal–Budapest Collaboration (stout smeared action) and that of the hotQCD Collaboration. The left panel is from Ref. [87] of the Wuppertal–Budapest Collaboration, the right panel is from the most recent hotQCD publication [91]. As can be seen, the results of the Wuppertal–Budapest Collaboration stayed constant in time, but the 40 MeV discrepancy, which had been there since 2006, disappeared recently.

In the above equation, X can be any quantity that has a dimension of mass. Since we are working with nonvanishing quark masses, m_π is a reasonable choice (another choice can be the temperature).

In order to compare our results to those of the hotQCD Collaboration, we also calculate the quantity $\Delta_{l,s}$ (strange subtracted chiral condensate), which is defined as

$$\Delta_{l,s} = \frac{\langle\bar{\psi}\psi\rangle_{l,T} - \frac{m_l}{m_s}\langle\bar{\psi}\psi\rangle_{s,T}}{\langle\bar{\psi}\psi\rangle_{l,0} - \frac{m_l}{m_s}\langle\bar{\psi}\psi\rangle_{s,0}} \quad l = u, d. \tag{3.4}$$

A comparison between our most recent [87] and earlier results [85,86] shows that our results did not change (only within error bars). The only change that can be observed was due to the change in the experimental f_K value in 2008, which resulted in a ≈ 6 MeV reduction of our T_c predictions (the dimensionless lattice results on T_c/f_K are unaltered).

As has already been mentioned, the most dramatic discrepancy was observed in quantities, which monitored the remnant of the chiral phase transition. The most precise observable, which can be directly compared for both of the collaborations, was the strange subtracted chiral condensate, which will be discussed below.

The two plots of Fig. 10 from the Wuppertal–Budapest group on the left and hotQCD on the right show the evolution of the transition temperature with essentially the same interpretations and conclusions. On the left (plot from Ref. [87] of the Wuppertal–Budapest Collaboration), the lower line shows the quite stable results of the Wuppertal–Budapest group from 2006. The hotQCD Collaboration used finer and finer lattices with smaller and smaller taste breaking and at the end the results of the two collaborations converged. On the right the same phenomenon is presented by the hotQCD Collaboration in their publication of Ref. [91]. The lower line is the continuum result of the Wuppertal–Budapest group and the red and blue points show how the hotQCD result approached the continuum one. It is a great success that two different actions converged to the same result and it contributed a lot to the credibility of lattice QCD outside the community.

3.3. Equation of state

Our collaboration presented two papers concerning the 2+1 flavor equation of state. The first paper [15] was written in 2005 and used physical quark masses on temporal extensions of 4 and 6. The

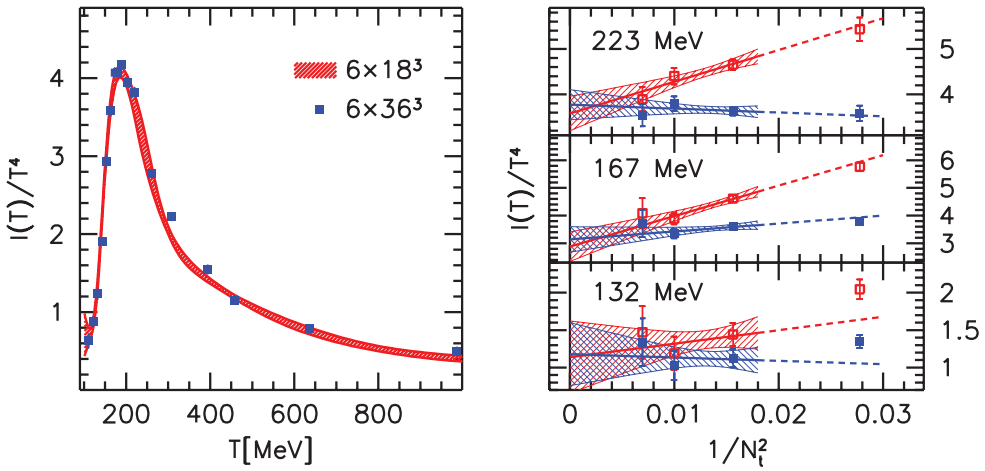

Fig. 11. Left panel: the trace anomaly on lattices with different spatial volumes: $N_s/N_t = 3$ (red band) and $N_s/N_t = 6$ (blue points). Right panel: the trace anomaly at three different temperatures as a function of $1/N_t^2$. Filled blue symbols represent the results within the lattice tree-level improvement framework, red open symbols show the results without this improvement. The error of the continuum extrapolated value is about 0.4 for all three temperatures.

second paper [92] appeared in 2010 and used temporal extensions 6, 8, 10 and, for three characteristic points (well above T_c, around T_c, and deep in the hadronic phase), temporal extensions of 12 were also used. Tree-level improvement factors were used for presenting the data. We have demonstrated that finite volume effects are negligible, as can be seen in the left panel of Fig. 11. We have also shown (see the right panel of the same figure) that, independently of the use of the improvement factors, the continuum extrapolated result is the same.

The basic quantity one determines to obtain the equation of state is the pressure. In the thermodynamic limit the pressure is related to the free energy density as

$$p = -\lim_{V\to\infty} f. \tag{3.5}$$

Having calculated the pressure (see Fig. 12) as a function of the temperature $p(T)$, all other thermodynamic observables can also be reconstructed. The trace anomaly $I = \epsilon - 3p$ is a straightforward derivative of the normalized pressure:

$$I = T^5 \frac{\partial}{\partial T} \frac{p(T)}{T^4}. \tag{3.6}$$

We parametrized the trace anomaly as a function of the temperature. We took the following fit function:

$$\frac{I(T)}{T^4} = \exp(-h_1/t - h_2/t^2) \cdot \left(h_0 + \frac{f_0 \cdot [\tanh(f_1 \cdot t + f_2) + 1]}{1 + g_1 \cdot t + g_2 \cdot t^2} \right), \tag{3.7}$$

where the dimensionless t variable is defined as $t = T/(200\,\mathrm{MeV})$. The parameters can be found in Table 2. This function reproduces the continuum estimate for the normalized trace anomaly in the entire temperature range $T = 100 \ldots 1000\,\mathrm{MeV}$. The $\{f_0, f_1, f_2\}$ parameters describe the steep rise of the trace anomaly in the transition region, whereas the $\{g_1, g_2\}$ parametrize the decrease for higher temperatures. The parametrization also approximates the hadron resonance gas (HRG) model prediction for $T < 100\,\mathrm{MeV}$; this is described by the $\{h_0, h_1, h_2\}$ parameters. For these temperatures the difference in the trace anomaly between the parametrization and the HRG model is less

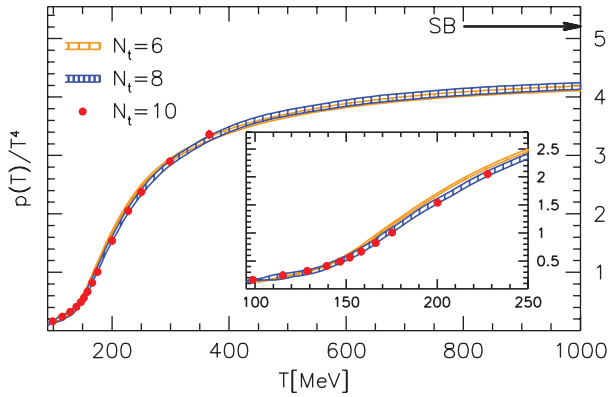

Fig. 12. The pressure normalized by T^4 as a function of the temperature on $N_t = 6, 8$, and 10 lattices. The Stefan–Boltzmann limit $p_{\rm SB}(T) \approx 5.209 \cdot T^4$ is indicated by an arrow. For our highest temperature $T = 1000\,\text{MeV}$ the pressure is almost 20% below this limit.

Table 2. Parameters of the function in Eq. (3.7) describing the trace anomaly in the $n_f = 2 + 1$ and $n_f = 2 + 1 + 1$ flavor cases. Note that the first three entries are the same (in the low temperature region the contribution of the charm is negligible).

h_0	h_1	h_2	f_0	f_1	f_2	g_1	g_2
0.1396	−0.1800	0.0350	2.76	6.79	−5.29	−0.47	1.04
0.1396	−0.1800	0.0350	5.59	7.34	−5.60	1.42	0.50

than $\Delta(I(T)/T^4) \leq 0.07$. From this parametrization the normalized pressure can be obtained by the definite integral

$$\frac{p(T)}{T^4} = \int_0^T \frac{dT}{T} \frac{I(T)}{T^4}. \tag{3.8}$$

The function obtained in this way goes through the points of the continuum estimate of the pressure for temperatures $T = 100 \ldots 1000\,\text{MeV}$, and for $T < 100\,\text{MeV}$ the deviation from the HRG prediction is less than $\Delta(p(T)/T^4) \leq 0.02$.

Using the pressure and the trace anomaly, the energy density ϵ, the entropy density s, and the speed of sound c_s can be calculated as

$$\epsilon = I + 3p, \quad s = \frac{\epsilon + p}{T}, \quad c_s^2 = \frac{dp}{d\epsilon}. \tag{3.9}$$

A central statement of our collaboration since 2005 is the height of the trace anomaly. Our prediction was always around 4, whereas the hotQCD results were—depending on the action—70, 50, or 40% higher. This can be clearly seen in both panels of Fig. 13. In the right panel, the parametrization s95p-v1p is also shown. This parametrization combines lattice QCD results of the hotQCD Collaboration at high temperatures [83,94] with the HRG model at low temperatures ($T < 170\,\text{MeV}$) [95]. The discrepancy between the two collaborations is obvious. Note, however, that it does not only appear in the peak height. It is instructive to compare (see Fig. 14) the entropy densities for the two parametrizations (Wuppertal–Budapest and the s95p-v1p, which is based on the hotQCD data and HRG at low temperatures). Since the Wuppertal–Budapest parametrization is better than the errors and the points are lying just on top of each other, we show these results and the result of the g^5 perturbation theory. As it can be seen, the Wuppertal–Budapest results are in quite good agreement with perturbation theory, whereas the s95p-v1p overshoots it. The resolution of the discrepancy between the Wuppertal–Budapest result and that of hotQCD remains a task for the future.

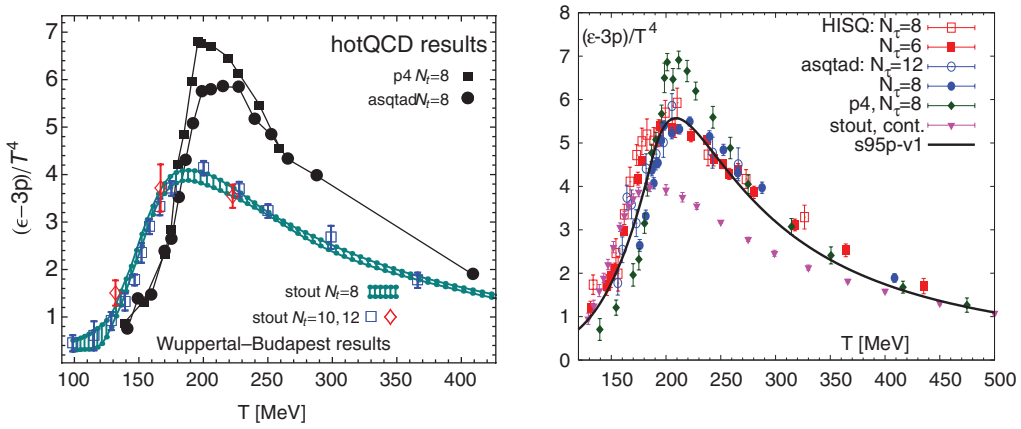

Fig. 13. Comparison of the trace anomaly for 2+1 flavour QCD for the Wuppertal–Budapest Collaboration (stout smeared action) and that of the hotQCD Collaboration. The left panel is from Ref. [92] of the Wuppertal–Budapest Collaboration, the right panel is from the most recent summary by a hotQCD Collaboration member [93]. The conclusions and interpretations are the same. The results of the Wuppertal–Budapest Collaboration stayed constant as N_t grew. The results of the hotQCD Collaboration change as their lattice resolution and/or taste violation improve. For example, the heights of the peak—depending on the hotQCD action and lattice spacing—are 70, 50, or 40% higher than those of the Wuppertal–Budapest prediction (green/blue and red symbols on the left and magenta points on the right).

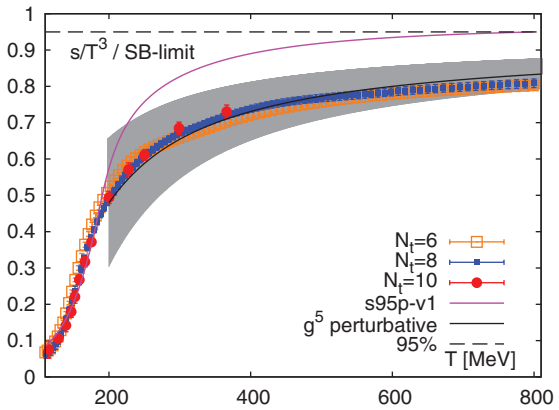

Fig. 14. Comparison of the temperature dependence of the entropy. The magenta line (s95p-v1p parametrization, which is based on the hotQCD data and HRG at low temperatures) reaches 95% of the Stefan–Boltzmann limit at 800 MeV. The Wuppertal–Budapest data, which are in good agreement with the perturbative prediction, are still 20% away from it at this temperature.

The Wuppertal–Budapest Collaboration determined the continuum limit of various quark number susceptibilities with physical quark masses [96]. We determined diagonal and nondiagonal quark number susceptibilities in a temperature range between 125 and 400 MeV. These calculations are particularly precise, since we used temporal lattice extensions from 6 up to 16 and the number of trajectories that were generated for each point were quite often beyond 100 000 (see Fig. 15).

All observables consistently show very good agreement with the HRG model predictions for temperatures below the transition.

The diagonal fluctuations have some common features: they all show a rapid rise in the crossover region, and reach approximately 90% of the corresponding ideal gas value at large temperatures. The rise of both strange quark and baryon number susceptibilities is shifted to temperatures about 20 MeV

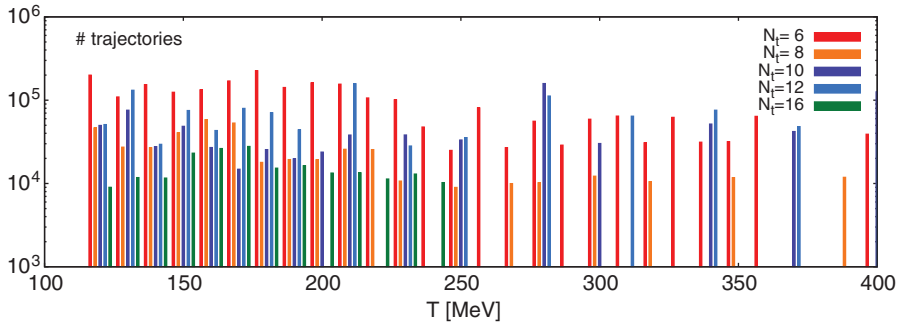

Fig. 15. The statistics used in this study. The number of trajectories exceeds 10^5 for several temperatures. Each bar refers to the respective color-coded lattice resolution in a 10 MeV wide temperature bin. We analyzed the gauge configurations after every tenth trajectory with 128 pairs of random sources (256 at $N_t = 16$) with the same physical quark masses that we had in the simulation.

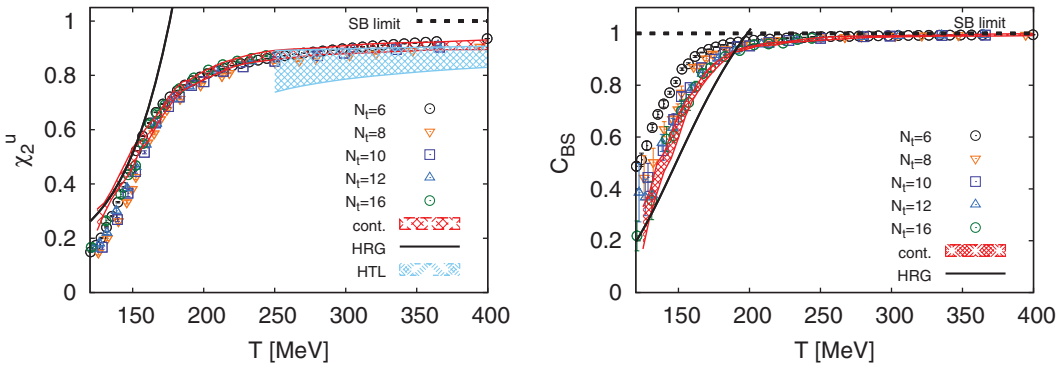

Fig. 16. Left panel: diagonal light quark susceptibility as a function of the temperature. Right panel: baryon–strangeness correlation as a function of the temperature. In both panels, the different symbols correspond to different N_t values. The red band is the continuum extrapolation. The black curve is the HRG model prediction for these observables. The dashed line shows the ideal gas limit. The light blue band in the left panel is the hard thermal loop (HTL) prediction taken from Ref. [97].

higher than those for light quark, charge, and isospin susceptibilities. Nondiagonal flavor and charge correlators remain different from their ideal gas values for a certain window of temperatures above the transition.

Two illustrative results (light quark susceptibility and the baryon–strangeness correlation) of this calculation can be seen in Fig. 16.

Finally, it is worth mentioning that we also calculated bulk observables with Wilson fermions around the transition region and extrapolated them to the continuum limit [98]. Results at two lattice spacings with overlap fermions were also obtained [99]. For the pure gauge theory, continuum results were presented for the equation of state in a wide temperature range [100]. These results are very important from a conceptual point of view: results with Wilson fermions confirmed earlier findings of staggered analyses, overlap results are approaching the continuum predictions using staggered fermions, and the pure SU(3) gauge theory closes the gap between lattice gauge theory and the perturbative approach. Since these calculations do not belong to the physical point calculations (physical quark masses extrapolated to the continuum limit) they will be discussed only briefly.

The Wilson results were obtained using pion masses of 545 MeV. Though this is far from the physical value, it is desirable to obtain continuum QCD results from first principles that do not contain

theoretically not fully justified operations such as the fourth root trick of rooted staggered fermions. The Wilson fermion formulation is theoretically sound and is known to be in the right universality class for QCD.

It seems logical to use chiral fermions to study chiral properties at finite temperature. Even though lattice chiral fermions are computationally much more expensive than the other types of discretization, they are advantageous for many reasons. Thus, we studied QCD thermodynamics using two flavors of dynamical overlap fermions with quark masses corresponding to a pion mass of 350 MeV. We determined several observables on $N_t = 6$ and 8 lattices. All our runs were performed with fixed global topology. Our results were compared with staggered ones and a nice agreement was found.

We presented the equation of state (pressure, trace anomaly, energy density, and entropy density) of the SU(3) gauge theory from lattice field theory in an unprecedented precision and temperature range. We control both finite size and cut-off effects. We determined the unknown g^6 order perturbative coefficient at extremely high temperatures. The high-precision data allow one to have a complete theoretical description of the equation of state from $T = 0$ all the way to the phase transition, through the transition region into the perturbative regime up to the Stefan–Boltzmann limit.

4. Nonvanishing chemical potentials and magnetic fields

In this section two major questions will be discussed. First we turn to a baryonic chemical potential (μ) and study its effect on the phase diagram and on the equation of state. Since the fermion determinant is not necessarily positive definite at a nonvanishing chemical potential, this physical situation is a particularly difficult one to study theoretically. The infamous sign problem spoils any lattice technique based on importance sampling. This difficulty slowed down the technical evolution of lattice QCD studies at $\mu > 0$. Nevertheless, renewed interest started [101] about a decade ago and today we even have a few continuum results, too (for a recent review, see, e.g., Ref. [102]). The other physically interesting question is related to nonvanishing magnetic fields. As we will see, they lead to a significant decrease of the transition temperature. As in all of the previous sections, only the results that were obtained for physical quark masses in the continuum limit are discussed in detail.

4.1. Lattice QCD at nonvanishing chemical potentials

In continuum we use the grand canonical potential to treat nonzero chemical potentials and use the corresponding μN term (N is the particle number). In the Euclidean lattice formulation the particle number is proportional to $\bar{\psi}\gamma_4\psi$. Thus, the most obvious solution for nonzero chemical potentials would be to add a $\mu \sum_x \bar{\psi}\gamma_4\psi$ term to the action. It is easy to show that this choice leads to a quadratic divergence. Note, however, that a term of the form $\mu \sum_x \bar{\psi}\gamma_4\psi$ corresponds to a constant purely imaginary vector potential. Since we describe gauge fields by link variables, it is straightforward to define nonvanishing chemical potentials by link variables too. Based on these ideas, it is clear how to introduce μ on the lattice. We multiply the forward timelinks $U_{x;4}$ by $e^{a\mu}$ and the backward timelinks $U^{\dagger}_{x;4}$ by $e^{-a\mu}$, otherwise the form of the action remains the same.

At nonvanishing chemical potentials we are faced with two serious problems. At zero chemical potential the positivity of the fermionic determinant is guaranteed by the γ_5 hermiticity of the fermion matrix. Unfortunately, at nonvanishing chemical potentials the γ_5 hermiticity is no longer fulfilled, and the fermion determinant can take complex values. The partition function and the observables are

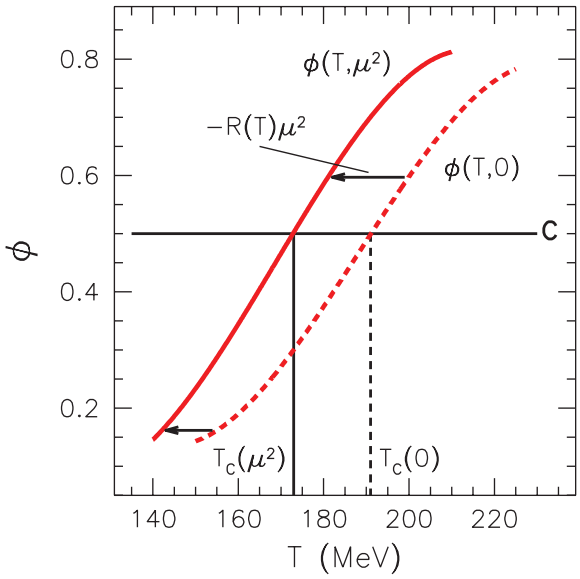

Fig. 17. Illustration of the behavior of the observable ϕ at $\mu = 0$ and $\mu > 0$. The quantity $T_c(\mu^2)$ is defined as the temperature where $\phi(T, \mu^2)$ crosses a constant value C. For $\mu > 0$, each point of the $\phi(T, 0)$ curve shifts in T by $R(T) \cdot \mu^2$ (see definition in text).

real valued, thus we can take the real part of the integrand $\Re \det M e^{-S_g}$. The positivity of this quantity is, however, not guaranteed: it can take both positive and negative values. This is the so-called sign problem.

This feature (positive and negative signs in the integrand) has two consequences. The more serious one is the impossibility of generating configurations based on importance sampling (a function with negative values cannot be interpreted as a probability distribution). The other problem is related to the cancellation due to contributions of different signs. Even if we could generate the necessary configurations, the sign of $\Re \det M e^{-S_g}$ for the individual configurations oscillates, and there are large cancellations in the average, which reduces the numerical accuracy.

As we have seen, the transition at $\mu = 0$ is a crossover [79] and we expect that the transition temperature decreases as we increase μ. Besides the actual value of the curvature of the transition line, a particularly interesting question is whether the transition becomes weaker or stronger as μ grows. A strengthening of the transition could lead to the existence of a critical point, as was observed on coarse lattices [103,104] (note that these calculations at $a = 0.3$ fm should be repeated with a controlled continuum extrapolation, a vital task for the future). The only continuum result concerning the phase diagram with physical quark masses is its curvature [105]. This calculation followed a truncated version of the multiparameter reweighting technique [101], which is called the Taylor method [106–108].

Parametrizing the transition line in the vicinity of the vertical $\mu = 0$ axis as

$$T_c(\mu^2) = T_c(1 - \kappa \cdot \mu^2 / T_c^2), \tag{4.1}$$

we look for the shift of T_c when μ increases. The temperature dependence of a given observable ϕ is given by $\phi(T)$. The function $R(T)$ is related to the shift of the $\phi(T)$ curve along the T axis as the chemical potential is varied. Given $\phi(T)$ and $R(T)$ at zero chemical potential, the shift for nonzero μ at leading order is $R(T) \cdot \mu^2$ (the curve moves to the left if $R(T)$ is negative and to the right otherwise). This behavior is illustrated in Fig. 17. Using $R(T)$ we can define a temperature-dependent

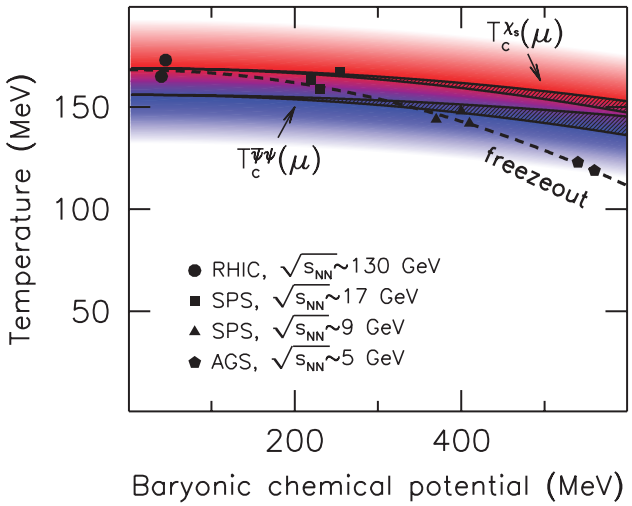

Fig. 18. The crossover transition between the 'cold' and 'hot' phases is represented by the colored area (blue and red correspond to the transition regions obtained from the chiral condensate and the strange susceptibility, respectively). The lower solid band shows the result for $T_c(\mu)$ defined through the chiral condensate and the upper one through the strange susceptibility. The widths of the bands represent the statistical uncertainty of $T_c(\mu)$ for the given μ coming from the error of the curvature κ for both observables. The dashed line is the freeze-out curve from heavy ion experiments [109]. Also indicated, with different symbols. are the individual measurements of the chemical freeze-out from RHIC, SPS (super proton synchrotron), and AGS (alternating gradient synchrotron), respectively. The center of mass energies $\sqrt{s_{NN}}$ for each are shown in the legend.

curvature according to (4.1) as $\kappa(T) = -T_c \cdot R(T)$. The meaning of $\kappa(T)$ is again simple: it gives the curvature of the $\phi =$ const. curve which starts from T at $\mu = 0$.

We studied the T dependence of the chiral condensate and the strange quark number susceptibility. The LCP was fixed by setting the ratios m_K/f_K and m_K/m_π to their physical values. We used three different lattice spacings $N_t = 6, 8, 10$ and aspect ratios N_s/N_t of 4 and 3. The scale was fixed by f_K and its unambiguity was checked by calculating m_{K*}, f_π, and r_0. The measurements were performed on clusters equipped with graphics cards [88]. Our final results are $\kappa^{(\chi_s/T^2)} = 0.0089(14)$ and $\kappa^{(\bar{\psi}\psi_r)} = 0.0066(20)$. We also obtained results for the widths and their temperature dependence. These results suggest that the transition remains a weak crossover with essentially constant strength for small to moderate chemical potentials. Actually, there is a slight increase in the width of the transition determined from both quantities. This effect is, however, very weak: the width only changes by a few percent up to $\mu \approx T_c$. One has to emphasize that all these findings were obtained in order μ^2. Higher orders can change the picture, particularly for moderate and large chemical potentials.

Our final result is shown in Fig. 18. The crossover region's extent changes little as the chemical potential increases, and within it two definitions give different curves for $T_c(\mu)$. It is useful to compare the whole picture to the freeze-out curve [109], which summarizes experimental results on the $\{T, \mu\}$ points where hadronization of the quark–gluon plasma was observed. This curve is expected to lie in the interior of the crossover region, as is also indicated by our results.

It is also possible to determine the equation of state at nonvanishing chemical potential with physical quark masses extrapolated in the continuum limit [110]. In this paper we determined the QCD equation of state for small chemical potentials using a Taylor-expansion technique. We employed $2 + 1$ flavors of quarks with physical masses and estimated the continuum limit of our data using lattices with $N_t = 6$, 8, 10, 12, and 16. We presented results regarding various thermodynamic observables as functions of the temperature and the 'light' baryonic chemical potential μ_L, which is

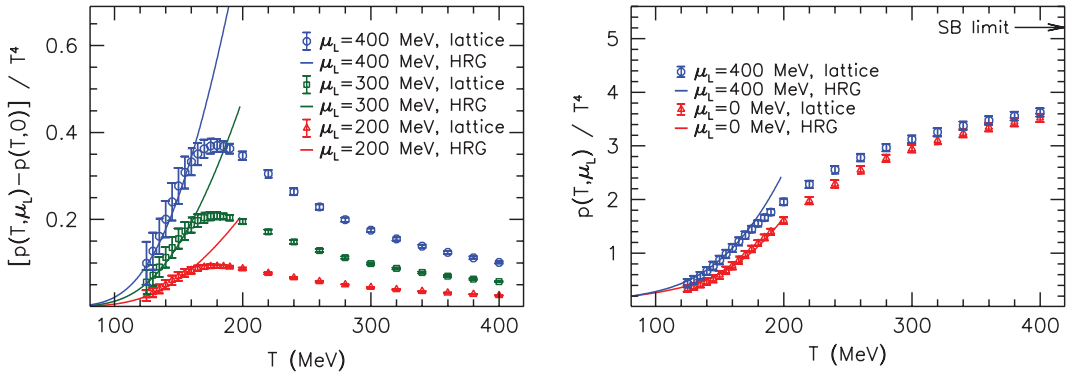

Fig. 19. The difference between the pressure at $\mu > 0$ and at $\mu = 0$ (left panel). The pressure for nonzero μ as a function of T (right panel).

the relevant parameter for the description of heavy ion collisions with zero net strangeness density. We also determined the isentropic equation of state and showed the observables along lines of constant entropy over particle number. A global parametrization of our observables was given such that they can be reconstructed for small chemical potentials $\mu_L/T_c = 3\mu_u/T_c \lesssim 3$ in the temperature window $0 < T < 400$ MeV. An illustrative example of our findings is shown in Fig. 19.

4.2. QCD thermodynamics at nonvanishing magnetic fields

Strong (electro)magnetic fields prominently feature in various physical systems. They play an essential role in cosmology, where magnetic fields of 10^{14} T and 10^{19} T may have been present [111,112] during the strong and electroweak phase transitions of the universe, respectively. Magnetic fields with strengths up to $B \sim 10^{14-16}$ T ($\sqrt{eB} \sim 0.1-1.0$ GeV) are also generated in noncentral heavy ion collisions [113–116] at the Relativistic Heavy Ion Collider (RHIC) or the Large Hadron Collider (LHC). Furthermore, for certain classes of neutron stars like magnetars, magnetic fields of the order of 10^{10} T have been deduced [117]. In addition to this phenomenological relevance, external (electro)magnetic fields can be used to probe the dynamics of strongly interacting matter, i.e. the vacuum structure of quantum chromodynamics (QCD).

As we have already discussed, one of the most important aspects of QCD is chiral symmetry breaking. At zero quark masses the chiral condensate $\bar{\psi}\psi$ is an order parameter. It vanishes at high temperatures where chiral symmetry is restored but develops a nonzero expectation value in the hadronic phase. It is an approximate order parameter for physical quark masses.

In the response of QCD to external magnetic fields, 'magnetic catalysis' refers to an increase of the condensate with B. This implies a B-dependence of T_c as well. Almost all low-energy models (see our recent paper, Ref. [118], for an extended reference list) and approximations to QCD as well as lattice simulations in quenched theories [119,120] at larger than physical pion masses in $N_f = 2$ QCD [121] and in the $N_f = 4$ SU(2) theory [122] found $\bar{\psi}\psi(B)$ and $T_c(B)$ to increase with B. In contrast, our large-scale study of QCD in external magnetic fields with physical pion mass $M_\pi = 135$ MeV and results extrapolated to the continuum limit [123] has revealed the transition temperature to *decrease* as a function of the external magnetic field. This applies to the T_c values defined from the quark condensate, the strange quark number susceptibility, and the chiral susceptibility. In particular, we found the condensate to depend on B in a *non-monotonous* way in the crossover region.

In this large scale simulation study [123], we considered $N_f = 1 + 1 + 1$ flavors on the lattice in the staggered fermionic formulation. A stout smeared Dirac operator is used, with physical quark

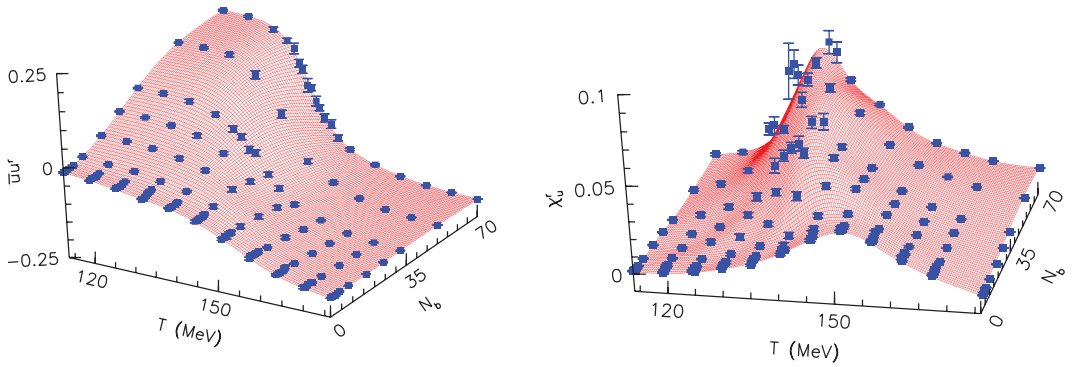

Fig. 20. The renormalized up quark condensate (left panel) and its susceptibility (right panel) as functions of T and N_b on our $N_t = 6$ lattices. Measurements are denoted by the blue points, while the red surface is the spline fit to the data.

masses (this is the same setup as in our other staggered thermodynamics studies). To study thermodynamics in a nonzero external field we analyze the chiral condensates and chiral susceptibilities for the light flavors $f = u, d$ and the strange quark number susceptibility

$$\bar{\psi}\psi_f \equiv \frac{T}{V}\frac{\partial \log \mathcal{Z}}{\partial m_f}, \quad \chi_f \equiv \frac{T}{V}\frac{\partial^2 \log \mathcal{Z}}{\partial m_f^2}, \quad c_2^s \equiv \frac{T}{V}\frac{1}{T^2}\frac{\partial^2 \log \mathcal{Z}}{\partial \mu_s^2}. \tag{4.2}$$

To take the continuum limit, renormalization of these observables has to be carried out. The logarithm of the partition function $\log \mathcal{Z}$ (i.e. the free energy) at $B = 0$ contains additive divergences of the forms a^{-4}, m^2a^{-2}, and $m^4 \log(a)$ [124]. It can be shown that there are no additional B-dependent divergences (the proof is based on the U(1) Ward identity [123]). Therefore the additive divergences of the observables derived from the free energy can be eliminated by subtracting the $T = 0$, $B = 0$ contribution. In the chiral quantities there are also multiplicative divergences caused by the derivative with respect to the quark mass. To eliminate this multiplicative divergence in the chiral condensate (susceptibility), we multiply by the first (second) power of the bare quark mass (the same procedure was applied in the previous sections). Finally, to obtain a dimensionless combination, we divide by the fourth power of the $T = 0$ pion mass m_π^4,

$$\begin{aligned} \bar{\psi}\psi_f^r(B,T) &= m_f[\bar{\psi}\psi_f(B,T) - \bar{\psi}\psi_f(B=0,T=0)]\frac{1}{m_\pi^4}, \\ \chi_f^r(B,T) &= m_f^2[\chi_f(B,T) - \chi_f(B=0,T=0)]\frac{1}{m_\pi^4}. \end{aligned} \tag{4.3}$$

Note that this procedure leads to a renormalized condensate that, for $B = 0$, is zero at $T = 0$ and approaches a negative value as T is increased. Considering the strange quark number susceptibility, c_2^s needs no renormalization (either at $B = 0$ or at $B \neq 0$) since it is connected to a conserved current.

We generated lattice configurations both at $T = 0$ and $T > 0$ with an exact RHMC algorithm, for various values of the gauge coupling and the magnetic flux. (To discretize the external magnetic field, the smeared links are multiplied by the U(1) links.) For the finite temperature runs we had lattice configurations with $N_t = 6, 8$, and 10. Finite volume effects are studied on the $N_t = 6$ ensemble using sets of $N_s = 16$, 24, and 32 lattices. The masses of the up, down, and strange quarks are set to their physical values along the line of constant physics (LCP) by fixing the ratios f_K/M_π and f_K/M_K to their experimental values. The lattice spacing is determined by f_K.

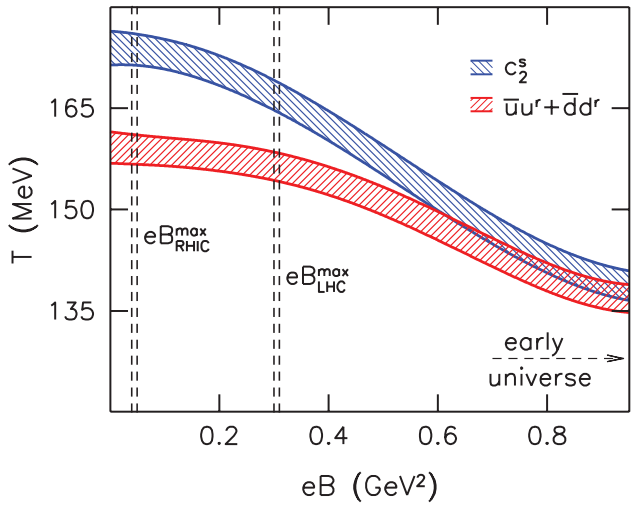

Fig. 21. Our final result for the QCD phase diagram in the magnetic field–temperature plane. The colored bands represent the pseudocritical temperature as defined from inflection points of the renormalized chiral condensate $\bar{u}u^r + \bar{d}d^r$ (red) and the strange quark number susceptibility c_2^s (blue) in the continuum limit. Also indicated by the dashed vertical lines are the maximal magnetic fields produced at RHIC and at the LHC. The large B region of the phase diagram is relevant for the evolution of the early universe.

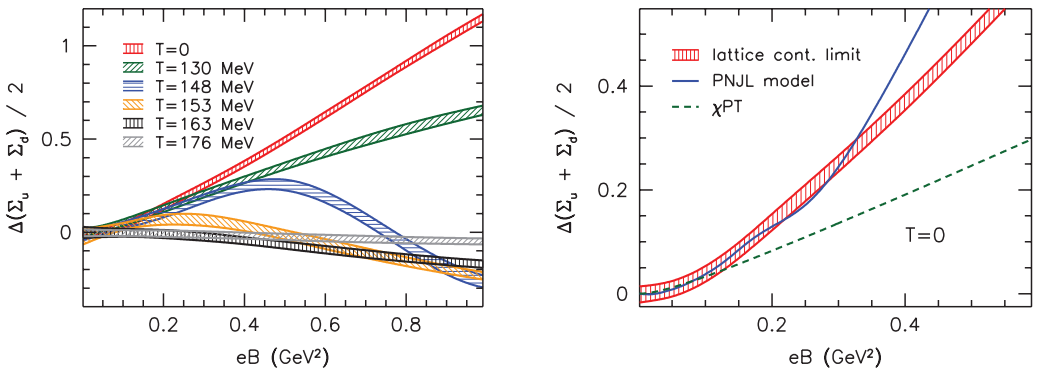

Fig. 22. Left panel: continuum extrapolated lattice results for the change of the condensate as a function of B, at six different temperatures. Right panel: comparison of the continuum limit of the change of the condensate to the χPT calculations [125–127] and the Polyakov-Nambu-Jona-Lasinio model [128] predictions.

We measured the observables discussed above. To determine them along a constant B line, interpolation is necessary, since magnetic flux N_b is quantized: $qB \cdot a^2 = 2\pi N_b/(N_x N_y)$. To this end we used a 2D spline function (see Fig. 20 for the renormalized up quark condensate and its susceptibility).

Finally, using the fitted 2D surfaces, we studied the observables as functions of temperature, along the lines of constant magnetic field. In particular, we analyzed the renormalized chiral susceptibility $\chi_u^r + \chi_d^r$, the renormalized chiral condensate $\bar{u}u^r + \bar{d}d^r$, and the strange quark number susceptibility c_2^s. For the latter two observables we determine the pseudocritical temperature $T_c(B)$ as the inflection points of the curves, while for the former we calculate the position of the maximum value of the observable. Our final results for the phase diagram are shown in Fig. 21.

In addition we determined the QCD light quark condensates at nonzero external magnetic field strengths for physical quark masses in the continuum limit for various temperatures (see Fig. 22).

Our results are in quantitative agreement with chiral perturbation theory and Polyakov-Nambu-Jona-Lasinio model predictions for small magnetic fields and at small temperatures. Note that the constants within these parametrizations have not been adjusted to our data but were taken from the literature where they have been obtained at vanishing magnetic field. Unsurprisingly, χPT fails in regions where pions cease to be the essential low energy degrees of freedom. While in the hadronic phase low energy models qualitatively reproduce the B-dependence of the lattice data, they miss an important feature that becomes dominant for light quark masses and for temperatures around T_c, as can be seen in Fig. 22.

5. Summary

In this paper some recent full results of the Budapest–Marseille–Wuppertal Collaboration have been summarized. Both $T = 0$ (light hadron spectrum, F_K/F_π, quark masses, B_K) and $T > 0$ findings (T_c, equation of state both at vanishing and nonvanishing chemical potentials or magnetic fields, and various fluctuations) have been presented. All results were obtained with physical quark masses and with continuum extrapolations. For the $T = 0$ studies, we typically used Wilson fermions, whereas, for thermodynamics, mostly staggered fermions were applied. Both fermion formulations have their advantages and disadvantages. (For a full comparison—physical quark masses with continuum extrapolations—on the 1% level we refer the reader to Ref. [129]), in which a scale variable was determined with both fermion formulations and complete agreement was found.) Full results are becoming the standard in lattice QCD, which signals a new era for our field.

Acknowledgements

The author thanks the members of the Budapest–Marseille–Wuppertal Collaboration for the enjoyable and successful collaborative work. Special thanks go to S.D. Katz for carefully reading this manuscript and for his suggestions. This work was partially supported by the DFG grant SFB/TR 55.

References

[1] K. G. Wilson, Phys. Rev. D **10**, 2445 (1974).
[2] K. G. Wilson, Nucl. Phys. Proc. Suppl. **140**, 3 (2005).
[3] I. Montvay and G. Munster, *Quantum Fields on a Lattice (Cambridge Monographs on Mathematical Physics)* (Cambridge University Press, Cambridge, UK, 1997).
[4] R. Gupta, arXiv:hep-lat/9807028.
[5] M. Di Pierro, arXiv:hep-lat/0009001.
[6] J. Smit, *Introduction to Quantum Fields on a Lattice (Cambridge Lecture Notes in Physics)* (Cambridge University Press, Cambridge, UK, 2002), p. 1.
[7] H. J. Rothe, World Sci. "Lecture Notes in Physics", **82**, 1 (2012).
[8] T. DeGrand and C. E. Detar, *Lattice Methods for Quantum Chromodynamics* (World Scientific, Hackensack, NJ, 2006).
[9] C. Gattringer and C. B. Lang, "Lecture Notes in Physics", **788**, 1 (2010).
[10] M. Creutz, *Quarks, Gluons and Lattices (Cambridge Monographs on Mathematical Physics)* (Cambridge University Press, Cambridge, UK, 1985).
[11] G. Curci, P. Menotti, and G. Paffuti, Phys. Lett. B **130**, 205 (1983); **135**, 516 (1984) [erratum].
[12] M. Luscher and P. Weisz, Commun. Math. Phys. **97**, 59 (1985); **98**, 433 (1985) [erratum].
[13] P. Weisz, Nucl. Phys. B **212**, 1 (1983).
[14] C. Morningstar and M. J. Peardon, Phys. Rev. D **69**, 054501 (2004).
[15] Y. Aoki, Z. Fodor, S. D. Katz, and K. K. Szabo, J. High Energy Phys. **0601**, 089 (2006).
[16] S. Durr et al., Phys. Rev. D **79**, 014501 (2009).
[17] S. Durr et al., J. High Energy Phys. **1108**, 148 (2011).
[18] S. Durr et al., Science **322**, 1224 (2008).

[19] Z. Fodor and C. Hoelbling, Rev. Mod. Phys. **84**, 449 (2012).
[20] S. Aoki et al. [CP-PACS Collaboration], Phys. Rev. Lett. **84**, 238 (2000).
[21] S. Aoki et al. [CP-PACS Collaboration], Phys. Rev. D **67**, 034503 (2003).
[22] C. T. H. Davies et al. [HPQCD Collaboration, UKQCD Collaboration, and MILC Collaboration], Phys. Rev. Lett. **92**, 022001 (2004).
[23] S. Aoki et al. [PACS-CS Collaboration], Phys. Rev. D **79**, 034503 (2009).
[24] C. W. Bernard et al., Phys. Rev. D **64**, 054506 (2001).
[25] C. Aubin et al., Phys. Rev. D **70**, 094505 (2004).
[26] N. Ukita et al. [PACS-CS Collaboration], PoS **LAT2007**, 138 (2007).
[27] M. Gockeler et al. [QCDSF Collaboration and UKQCD Collaboration], PoS **LAT2007**, 129 (2007).
[28] D. J. Antonio et al. [RBC Collaboration and UKQCD Collaboration], Phys. Rev. D **75**, 114501 (2007).
[29] A. Walker-Loud et al., Phys. Rev. D **79**, 054502 (2009).
[30] L. Del Debbio, L. Giusti, M. Luscher, R. Petronzio, and N. Tantalo, J. High Energy Phys. **0702**, 056 (2007).
[31] C. Alexandrou et al. [European Twisted Mass Collaboration], Phys. Rev. D **78**, 014509 (2008).
[32] J. Noaki et al. [JLQCD Collaboration], PoS **LAT2007**, 126 (2007).
[33] M. Luscher, Commun. Math. Phys. **104**, 177 (1986).
[34] M. Luscher, Commun. Math. Phys. **105**, 153 (1986).
[35] M. Luscher, Nucl. Phys. B **354**, 531 (1991).
[36] M. Luscher, Nucl. Phys. B **364**, 237 (1991).
[37] G. Colangelo and S. Durr, Eur. Phys. J. C **33**, 543 (2004).
[38] K. Nakamura et al. [Particle Data Group], J. Phys. G **37**, 075021 (2010).
[39] S. Durr et al., Phys. Rev. D **81**, 054507 (2010).
[40] W. J. Marciano, Phys. Rev. Lett. **93**, 231803 (2004).
[41] J. Beringer et al. (Particle Data Group), Phys. Rev. D **86**, 010001 (2012).
[42] J. C. Hardy and I. S. Towner, Phys. Rev. C **79**, 055502 (2009).
[43] J. Gasser and H. Leutwyler, Nucl. Phys. B **250**, 465 (1985).
[44] C. Allton et al. [RBC-UKQCD Collaboration], Phys. Rev. D **78**, 114509 (2008).
[45] L. Lellouch, PoS **LATTICE2008**, 015 (2009).
[46] M. Antonelli et al. [FlaviaNet Working Group on Kaon Decays], arXiv:0801.1817 [hep-ph].
[47] H. Fritzsch, M. Gell-Mann, and H. Leutwyler, Phys. Lett. B **47**, 365 (1973).
[48] M. Creutz, Phys. Rev. D **21**, 2308 (1980).
[49] J. Garden, J. Heitger, R. Sommer, and H. Wittig [ALPHA Collaboration and UKQCD Collaboration], Nucl. Phys. B **571**, 237 (2000).
[50] C. W. Bernard and M. F. L. Golterman, Phys. Rev. D **46**, 853 (1992).
[51] S. R. Sharpe, Phys. Rev. D **46**, 3146 (1992).
[52] N. Eicker et al. [TXL Collaboration], Phys. Lett. B **407**, 290 (1997).
[53] A. Ali Khan et al. [CP-PACS Collaboration], Phys. Rev. D **65**, 054505 (2002); **67**, 059901 (2003) [erratum].
[54] S. Aoki et al. [JLQCD Collaboration], Phys. Rev. D **68**, 054502 (2003).
[55] M. Gockeler, R. Horsley, A. C. Irving, D. Pleiter, P. E. L. Rakow, G. Schierholz, and H. Stuben [QCDSF Collaboration and UKQCD Collaboration], Phys. Lett. B **639**, 307 (2006).
[56] M. Della Morte et al. [ALPHA Collaboration], Nucl. Phys. B **729**, 117 (2005).
[57] C. Aubin et al. [HPQCD Collaboration, MILC Collaboration, and UKQCD Collaboration], Phys. Rev. D **70**, 031504 (2004).
[58] A. Bazavov et al. [MILC Collaboration], PoS **LAT2009**, 079 (2009).
[59] A. Bazavov et al., Rev. Mod. Phys. **82**, 1349 (2010).
[60] C. T. H. Davies et al., Phys. Rev. Lett. **104**, 132003 (2010).
[61] C. McNeile, C. T. H. Davies, E. Follana, K. Hornbostel, and G. P. Lepage, Phys. Rev. D **82**, 034512 (2010).
[62] B. Blossier et al. [ETM Collaboration], Phys. Rev. D **82**, 114513 (2010).
[63] Y. Aoki et al. [RBC Collaboration and UKQCD Collaboration], Phys. Rev. D **83**, 074508 (2011).
[64] G. Colangelo et al., Eur. Phys. J. C **71**, 1695 (2011).
[65] S. Durr et al., Phys. Lett. B **701**, 265 (2011).
[66] T. Blum, R. Zhou, T. Doi, M. Hayakawa, T. Izubuchi, S. Uno, and N. Yamada, Phys. Rev. D **82**, 094508 (2010).

[67] S. Capitani, S. Durr, and C. Hoelbling, J. High Energy Phys. **0611**, 028 (2006).
[68] G. Martinelli, C. Pittori, C. T. Sachrajda, M. Testa, and A. Vladikas, Nucl. Phys. B **445**, 81 (1995).
[69] A. Donini, V. Gimenez, G. Martinelli, M. Talevi, and A. Vladikas, Eur. Phys. J. C **10**, 121 (1999).
[70] M. Ciuchini, E. Franco, V. Lubicz, G. Martinelli, I. Scimemi, and L. Silvestrini, Nucl. Phys. B **523**, 501 (1998).
[71] A. J. Buras, M. Misiak, and J. Urban, Nucl. Phys. B **586**, 397 (2000).
[72] J. Charles et al. [CKMfitter Group], Eur. Phys. J. C **41**, 1 (2005).
[73] P. de Forcrand, S. Kim, and O. Philipsen, PoS **LAT2007**, 178 (2007).
[74] G. Endrodi, Z. Fodor, S. D. Katz, and K. K. Szabo, PoS **LAT2007**, 182 (2007).
[75] F. Karsch, E. Laermann, and C. Schmidt, Phys. Lett. B **520**, 41 (2001).
[76] D. J. Schwarz, Ann. Phys. **12**, 220 (2003).
[77] E. Witten, Phys. Rev. D **30**, 272 (1984).
[78] J. H. Applegate and C. J. Hogan, Phys. Rev. D **31**, 3037 (1985).
[79] Y. Aoki, G. Endrodi, Z. Fodor, S. D. Katz, and K. K. Szabo, Nature **443**, 675 (2006).
[80] M. Cheng et al., Phys. Rev. D **74**, 054507 (2006).
[81] F. Karsch, PoS **LAT2007**, 015 (2007).
[82] F. Karsch [RBC Collaboration and HotQCD Collaboration], J. Phys. G **35**, 104096 (2008).
[83] A. Bazavov et al., Phys. Rev. D **80**, 014504 (2009).
[84] M. Cheng et al., Phys. Rev. D **81**, 054504 (2010).
[85] Y. Aoki, Z. Fodor, S. D. Katz, and K. K. Szabo, Phys. Lett. B **643**, 46 (2006).
[86] Y. Aoki, S. Borsanyi, S. Durr, Z. Fodor, S. D. Katz, S. Krieg, and K. K. Szabo, J. High Energy Phys. **0906**, 088 (2009).
[87] S. Borsanyi, Z. Fodor, C. Hoelbling, S. D. Katz, S. Krieg, C. Ratti, and K. K. Szabo [Wuppertal–Budapest Collaboration], J. High Energy Phys. **1009**, 073 (2010).
[88] G. I. Egri, Z. Fodor, C. Hoelbling, S. D. Katz, D. Nogradi, and K. K. Szabo, Comput. Phys. Commun. **177**, 631 (2007).
[89] N. Ishizuka, M. Fukugita, H. Mino, M. Okawa, and A. Ukawa, Nucl. Phys. B **411**, 875 (1994).
[90] G. Colangelo, S. Durr, and C. Haefeli, Nucl. Phys. B **721**, 136 (2005).
[91] A. Bazavov et al., Phys. Rev. D **85**, 054503 (2012).
[92] S. Borsanyi et al., J. High Energy Phys. **1011**, 077 (2010).
[93] P. Petreczky, arXiv:1203.5320 [hep-lat].
[94] M. Cheng et al., Phys. Rev. D **77**, 014511 (2008).
[95] P. Huovinen and P. Petreczky, Nucl. Phys. A **837**, 26 (2010).
[96] S. Borsanyi, Z. Fodor, S. D. Katz, S. Krieg, C. Ratti, and K. Szabo, J. High Energy Phys. **1201**, 138 (2012).
[97] J. P. Blaizot, E. Iancu, and A. Rebhan, Phys. Lett. B **523**, 143 (2001).
[98] S. Borsanyi et al., arXiv:1205.0440 [hep-lat].
[99] S. Borsanyi et al., Phys. Lett. B **713**, 342 (2012).
[100] S. Borsanyi, G. Endrodi, Z. Fodor, S. D. Katz, and K. K. Szabo, arXiv:1204.6184 [hep-lat].
[101] Z. Fodor and S. D. Katz, Phys. Lett. B **534**, 87 (2002).
[102] Z. Fodor and S. D. Katz, arXiv:0908.3341 [hep-ph].
[103] Z. Fodor and S. D. Katz, J. High Energy Phys. **0203**, 014 (2002).
[104] Z. Fodor and S. D. Katz, J. High Energy Phys. **0404**, 050 (2004).
[105] G. Endrodi, Z. Fodor, S. D. Katz, and K. K. Szabo, J. High Energy Phys. **1104**, 001 (2011).
[106] C. R. Allton et al., Phys. Rev. D **71**, 054508 (2005).
[107] R. V. Gavai and S. Gupta, Phys. Rev. D **78**, 114503 (2008).
[108] S. Basak et al. [MILC Collaboration], PoS **LATTICE2008**, 171 (2008).
[109] J. Cleymans and K. Redlich, Phys. Rev. Lett. **81**, 5284 (1998).
[110] S. Borsanyi, G. Endrodi, Z. Fodor, S. D. Katz, S. Krieg, C. Ratti, and K. K. Szabo, arXiv:1204.6710 [hep-lat].
[111] T. Vachaspati, Phys. Lett. B **265**, 258 (1991).
[112] K. Enqvist and P. Olesen, Phys. Lett. B **319**, 178 (1993).
[113] V. Skokov, A. Y. Illarionov, and V. Toneev, Int. J. Mod. Phys. A **24**, 5925 (2009).
[114] V. Voronyuk, V. D. Toneev, W. Cassing, E. L. Bratkovskaya, V. P. Konchakovski, and S. A. Voloshin, Phys. Rev. C **83**, 054911 (2011).
[115] A. Bzdak and V. Skokov, Phys. Lett. B **710**, 171 (2012).

[116] W. T. Deng and X. G. Huang, Phys. Rev. C **85**, 044907 (2012).
[117] R. C. Duncan and C. Thompson, Astrophys. J. **392**, L9 (1992).
[118] G. S. Bali, F. Bruckmann, G. Endrodi, Z. Fodor, S. D. Katz, and A. Schafer, arXiv:1206.4205 [hep-lat].
[119] P. V. Buividovich, M. N. Chernodub, E. V. Luschevskaya, and M. I. Polikarpov, Phys. Lett. B **682**, 484 (2010).
[120] V. V. Braguta, P. V. Buividovich, T. Kalaydzhyan, S. V. Kuznetsov, and M. I. Polikarpov, PoS **LATTICE2010**, 190 (2010).
[121] M. D'Elia and F. Negro, Phys. Rev. D **83**, 114028 (2011).
[122] E. M. Ilgenfritz, M. Kalinowski, M. Muller-Preussker, B. Petersson, and A. Schreiber, Phys. Rev. D **85**, 114504 (2012).
[123] G. S. Bali et al., J. High Energy Phys. **1202**, 044 (2012).
[124] H. Leutwyler and A. V. Smilga, Phys. Rev. D **46**, 5607 (1992).
[125] T. D. Cohen, D. A. McGady, and E. S. Werbos, Phys. Rev. C **76**, 055201 (2007).
[126] J. O. Andersen, arXiv:1202.2051 [hep-ph].
[127] J. O. Andersen, arXiv:1205.6978 [hep-ph].
[128] R. Gatto and M. Ruggieri, Phys. Rev. D **83**, 034016 (2011).
[129] S. Borsanyi et al., J. High Energy Phys. **1209**, 010 (2012).